

Topical Review

Rational design of nanoarray structures for lithium–sulfur batteries: recent advances and future prospects

Longtao Ren^{1,6}, Jun Liu^{1,6}, Abdul Hameed Pato¹, Yan Wang¹, Xiwen Lu¹, Imran Ali Chandio¹, Mingyue Zhou⁴, Wen Liu^{1,2,*}, Haijun Xu^{2,5,*} and Xiaoming Sun^{1,2,3}

¹ College of Chemistry, Beijing University of Chemical Technology, Beijing 100029, People's Republic of China

² State Key Laboratory of Chemical Resource Engineering, Beijing 100029, People's Republic of China

³ Beijing Advanced Innovation Center for Soft Matter Science and Engineering, Beijing 100029, People's Republic of China

⁴ Beijing Key Laboratory of Green Chemical Reaction Engineering and Technology, Department of Chemical Engineering, Tsinghua University, Beijing 100084, People's Republic of China

⁵ College of Mathematics and Physics, Beijing University of Chemical Technology, Beijing 100029, People's Republic of China

E-mail: wenliu@mail.buct.edu.cn and hjxu@mail.buct.edu.cn

Received 23 April 2023, revised 29 June 2023

Accepted for publication 17 July 2023

Published 25 August 2023



CrossMark

Abstract

Lithium–sulfur (Li–S) batteries are considered as promising candidates for future-generation energy storage systems due to their prominent theoretical energy density. However, their application is still hindered by several critical issues, e.g., the low conductivity of sulfur species, the shuttling effects of soluble lithium polysulfides, volumetric expansion, sluggish redox kinetics, and uncontrollable Li dendritic formation. Considerable research efforts have been devoted to breaking through the obstacles that are preventing Li–S batteries from realizing practical application. Recently, benefiting from the no additives/binders, buffer of volume change, high sulfur loading and suppression of lithium dendrites, nanoarray (NA) structures have emerged as efficient and durable electrodes in Li–S batteries. In this work, recent advances in the design, synthesis and application of NA structures in Li–S batteries are reviewed. First, the multifunctional merits and typical synthetic strategies of employing NA structure electrodes for Li–S batteries are outlined. Second, the applications of NA structures

⁶ These authors contributed equally to this work.

* Authors to whom any correspondence should be addressed.



Original content from this work may be used under the terms of the [Creative Commons Attribution 4.0 licence](https://creativecommons.org/licenses/by/4.0/). Any further distribution of this work must maintain attribution to the author(s) and the title of the work, journal citation and DOI.

in Li–S batteries are discussed comprehensively. Finally, the challenge and rational design of NA structure for Li–S batteries are analyzed in depth, with the aim of providing promising orientations for the commercialization of high-energy-density Li–S batteries.

Keywords: nanoarrays, electrocatalysts, surface and interface engineering, lithium–sulfur batteries, modulated strategies

1. Introduction

With the depletion of fossil fuels and ever-increasing demand for energy sources, it is crucial to develop sustainable energy resources and affordable energy storage technologies to resolve energy and environmental issues [1–5]. Over the past three decades, rechargeable lithium ion batteries (LIBs) have been widely used in a variety of applications such as portable electronics, electric vehicles, and even grid-scale energy storage [6, 7]. The widely commercialized LIBs comprised of conventional insertion cathode materials, such as LiCoO_2 and LiFePO_4 , have reached an energy density of around 200 Wh kg^{-1} [8–10]. Obviously, the limited energy density of conventional LIBs cannot meet the increasing energy density demand of modern society. In recent years, lithium–sulfur (Li–S) batteries have drawn significant attention and are recognized as potential future-generation energy storage systems due to their considerable theoretical specific energy of 2600 Wh kg^{-1} and the impressive specific capacity of 1675 mA h g^{-1} [11–13]. Most importantly, sulfur has the outstanding advantages of high natural abundance, low cost, and being eco-friendly, which in turn promotes the commercialization potential of Li–S batteries [14, 15].

Nevertheless, the commercial application of Li–S batteries is still impeded by several intrinsic demerits: (i) the intrinsically insulating nature of sulfur ($5 \times 10^{-30} \text{ S cm}^{-1}$ at 25°C) induces the low utilization of sulfur in the electrochemical reaction; (ii) the high solubility and shuttling effect of lithium polysulfide intermediates (Li_2S_x , $4 \leq x \leq 8$) in the electrolyte leads to the loss of active species and poor cycling performance; (iii) the huge volumetric expansion of sulfur ($\approx 80\%$) upon lithiation always causes the collapse of the sulfur cathode; and (iv) severe growth of Li-dendrites on the anode surface deteriorates the cycling life and even causes safety issues [16, 17]. To address these issues, numerous efforts have been devoted to the design and synthesis of various host materials for sulfur cathodes with different chemical compositions and structures [18–21]. On the other hand, some researchers are also focusing on electrolyte optimization, anode protection, and separator modification [22–25]. In the case of soluble lithium polysulfides, it is widely accepted that nanomaterials with the ‘quantum size effect’ can mitigate the shuttling effect as a physical barrier [22, 26]. Unfortunately, nanomaterials have more critical surface/interface issues, for instance, the high specific surface area generally results in particulate aggregation and irreversible surface side reactions. It is therefore imperative to rationally design the electrode structures and make optimal use of related surfaces and interfaces

in order to overcome the limitations of nanomaterials for energy storage.

More recently, nanoarrays (NAs) grown on different substrates (such as nickel foam, carbon paper and graphite felt) have shown great potential in energy storage due to their highly ordered structures [15, 27, 28] as well as their large surface areas. These unique structures have fully exposed, continuous, ordered active sites that can efficiently promote charge transfer across the electrode surface/interfaces. Here, we provide an overview of recent advances in the rational design and construction of NA structures for Li–S batteries (figure 1). This review will begin by summarizing and discussing a series of synthetic strategies for NA structures. We then provide a comprehensive coverage of the recent advances in NA structures for Li–S batteries and analyze their kinetic advantages for the optimization of the sulfur cathode, separator, and Li metal anode. Finally, we put forward the key to the rational design of NA structures and expound the opportunities and challenges for future research in Li–S batteries.

2. Main features and benefits of NAs in Li–S batteries

NAs are an ordered arrangement of nanorods, nanotubes, nanosheets or other independent structural elements of nanometer size that can be interdependent to create a physical and chemical synergistic effect and coupling effects [15, 29, 30]. NA structures offer integrated merits, including:

- (i) **Buffering the volume change.** The interval void between adjacent nanostructures effectively buffers the volume change of the active materials and helps to relax the stress [31].
- (ii) **Facilitating rapid electron transport and facile ion diffusion.** The conductive substrate provides a convenient direct electron pathway, thus facilitating charge transfer. In addition, the ordered mesoporous architecture of NAs offers facile ion diffusion routes, thus reducing the resistance of ion transport between the electrode and the electrolyte [32].
- (iii) **Improving the utilization of active materials.** Active materials are effectively immobilized on the surface of the ordered and separated arrayed architecture that is fully available for the electrochemical reaction [33].
- (iv) **More active sites and a more stable structure.** The high specific surface area and robust structure of

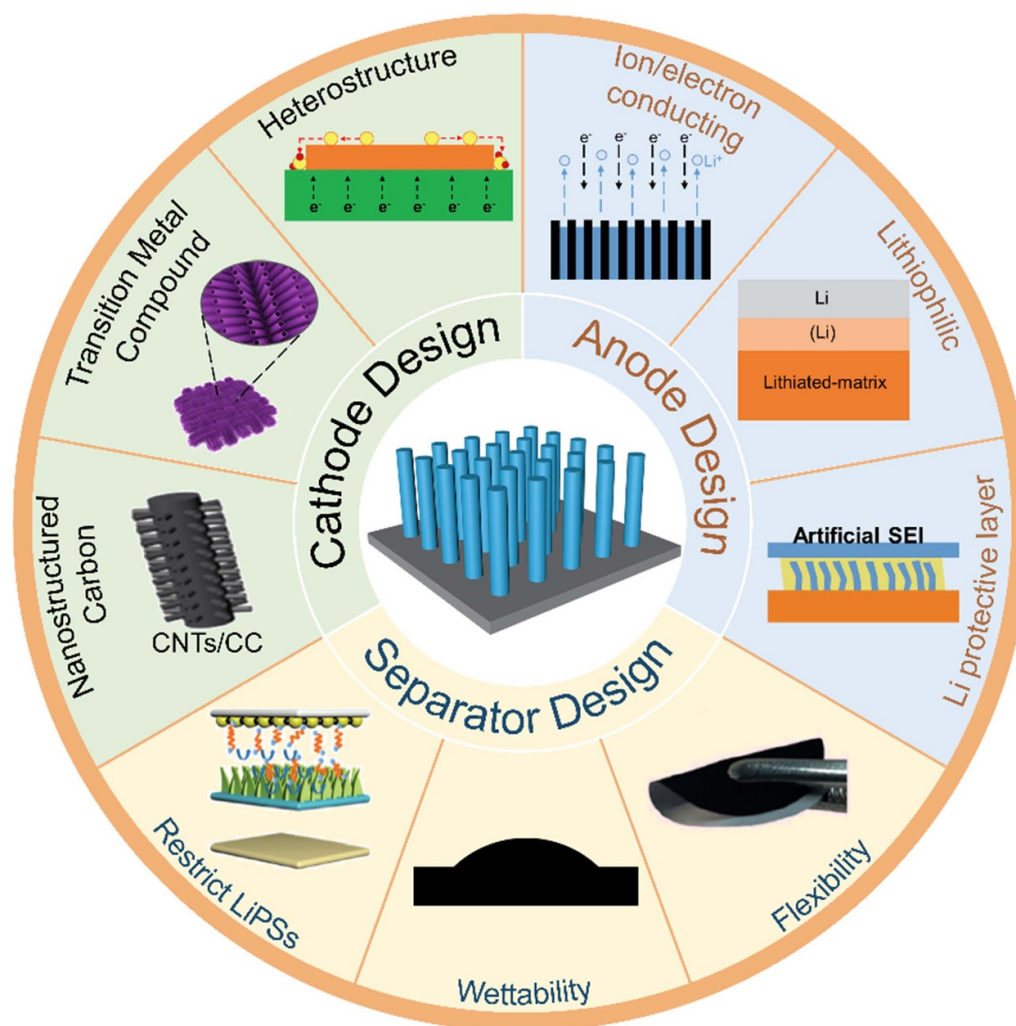


Figure 1. Schematic illustration of NA structures for Li–S batteries.

NAs providesubstantial contact between the electrode/ electrolyte and exposes more active sites [34].

Conventional sulfur cathodes are prepared by coating slurry onto the current collectors, where inert materials such as polymer binders and conductive additives take up a considerable percentage of the weight, resulting in a decrease of energy density [35]. Besides, the binders and additives will block some active sites from contacting with the electrolyte, leading to the incomplete utilization of active materials for electrochemical reaction. Furthermore, traditional slurry cast cathodes are not robust enough, loading large amounts of active materials, which may cause lots of cracks or the dropping of powder. Because of this, the sulfur loading amount is usually less than 4.0 mg cm^{-2} [36, 37]. In addition, the disordered surface and interface of powder cathodes increase the resistance to ionic and electronic transport and induce additional side reactions [38]. NA electrodes can be used to address the above issues. First, instead of adding polymer binders into the casting electrode, NA electrodes can be grown directly on conductive substrates, such as nickel foam, carbon cloth or paper, and metal foil. The ordered and separated arrays on the current

collector provide rapid electron transport pathways and facilitate ion diffusion routes; thus even a thick electrode can realize sufficient electrochemical utilization of the active materials. Second, the NA structures can effectively alleviate the stress caused by the volume change between S_8 and Li_2S , which improves the stability of the electrode material. Third, these robust and stable structures can easily achieve high sulfur loading. The voids between the vertically and orderly arranged NAs are conducive for molten sulfur or sulfur vapor penetration into the electrode, resulting in high sulfur loading in the composite cathode. Finally, this can greatly simplify electrode preparation, making it easier to industrialize Li–S batteries. In particular, the NA electrodes grown on flexible substrates can be used to realize flexible energy storage and conversion devices with excellent properties of flexibility, and being lightweight and portable [39–41].

For a Li metal anode, the unstable solid electrolyte interphase (SEI), infinite volume change and uncontrollable Li dendrite growth result in unstable Li stripping/plating [42]. Several emerging strategies have been investigated to enhance the electrochemical performance of a Li metal anode, including surface protection, host materials and solid

electrolyte [43–47]. One of these is the discovery that by forming a framework of ‘lithophilic’ NAs, the appearance of Li metal dendrites can be greatly reduced [48]. Therefore, the application of NAs structures in Li metal anodes is becoming increasingly compelling for a number of reasons: (i) the interconnect backbone of NAs with high electronic conductivity can provide a good electron transport pathway; (ii) the large surface area can effectively decrease the local current densities, and the diffusion barrier of Li ions can be significantly decreased; and (iii) the well-designed structure efficiently eliminates the notorious Lightning-Rod effect of Li anodes, leading to a smooth and dendrite free Li metal deposition [49–52].

3. Synthetic methods of NAs

3.1. Hydrothermal/solvothermal synthesis

One of the most popular approaches is the hydrothermal/solvothermal method, which involves heterogeneous reactions at elevated temperature and high pressure [53, 54]. Hydrothermal methods are typically used for some reactions that cannot easily occur at room temperature and normal pressure. The crystalline structure, morphology, and size of the products can also be well controlled by adjusting the reaction time, temperature and capping reagent [55, 56]. Therefore, the reactant and substrate are sealed in a Teflon-line sealed reactor, and the ideal crystalline material can be obtained after being kept at a certain temperature in an oven [57]. Currently, this method is often used to synthesize arrays of transition metal hydroxides, oxides, sulfides, and other metal compounds on metal and carbon substrates with on-site growth due to less particle agglomeration [54, 58].

Lu *et al* prepared the CoSO_4 hydrate nanomaterials with three kinds of morphologies through the control of the hydrothermal time required for vulcanization of the precursor [59]. Recently, Chen and coworkers prepared a flexible sulfur host material that is composed of FeCo_2S_4 nanotube arrays grown on the surface of carbon cloth via a two-step hydrothermal method (figures 2(a) and (b)) [60]. It is interesting to note that carbon cloth, as the conductive substrate in this process can not only act as a scaffold for the growth of nanostructured arrays, but also offers a binder-free cathode for Li–S batteries to effectively inhibit the shuttling effect. Dai *et al* used a one-step hydrothermal method to fabricate highly conductive honeycomb-like sulfiphilic spheres constructed from hollow, metallic, and polar Co_9S_8 tubules as a sulfur host [61]. The structure of the arrays allowed the nanomaterials to expose more catalytically active sites for better adsorption and catalytic conversion of polysulfides. Thus, the hydrothermal/solvothermal synthesis is a versatile approach to optimize the activity of NAs.

3.2. Chemical vapor deposition (CVD)

CVD is a process wherein a reactant vapor containing elements is introduced into a reaction chamber, facilitating chemical

reactions on the substrate surface and resulting in the formation of thin films. CVD can be applied to various base materials, offering strong adhesion. Additionally, it enables higher material deposition rates and achieves higher coating density. The size and microstructure of the deposited material can be controlled [62–64]. However, the high operating costs and low material utilization associated with this method restrict its widespread application in industrial processes.

For example, the $\text{Co}(\text{OH})_2$ nanowire array was first synthesized on carbon fiber paper (CFP) using a hydrothermal method (figure 2(c)). The treated CoO array was used as a template and pre-catalyst for the growth of CNTs that were synthesized using a CVD method thereafter. During the preparation process, ethanediamine was used as both C and N element source in order to investigate the sulfur confining effect of the designed NAs structure (figure 2(d)) [65]. MoS_2 – MoN heterostructure nanosheets were prepared by a CVD method to accelerate the conversion of polysulfides in Li–S batteries with high energy density [66]. For materials synthesis, a piece of MoS_2 host was placed in a quartz tube of a CVD furnace, then heated up to 800°C under Ar/NH_3 gas flow for 30 min. The combination of CVD and other preparation methods is used to achieve hierarchical structures and synergy of different compositions. Sun *et al* designed an array of nitrogen doped carbon nanotube (CNT) arrays (NTs) as a 3D conducting host, and VS_4 nanoparticles (VS@NT) are loaded uniformly through CVD and hydrothermal methods successively. The synergistic effect of the two materials has enabled the cell to achieve excellent electrochemical performance with a high rate capacity of up to 451 mA h g^{-1} at 6 C and excellent long cycle ability with a low decay rate of 0.037% per cycle up to 1200 cycles at 2 C [67].

3.3. Template synthesis

In some research, the template method is used to control the size, morphology, and structure of nanomaterials through spatial confinement effects [68, 69]. Template-directed (soft or hard template) synthesis is a more reliable and versatile synthetic technique for fabricating ordered 1D NAs, such as nanorods, nanowires, and nanotubes [70–72]. Most importantly, the template synthesis approach has the significant advantage of being independent of the materials’ lattice preference to achieve desirable nano-geometry.

Zhou and coworkers reported a highly conductive and flexible S-CNTs membrane derived from an aluminum oxide (AAO) template by using anodic AAO as a typical hard template (figures 2(e) and (f)). The nanostructured membrane was used as a self-supporting cathode without metal current-collectors in an Li–S coin cell [73]. As sulfur was confined within the walls of the CNTs, the dissolution of lithium polysulfides was restricted, offering the material a long cycle life. Beyond AAO templates, ZnO materials are also commonly used as templates for the synthesis of nanostructured arrays [74]. The 3D ZnO nanorods array acts as a template that is etched during the formation of the carbon nanorods array. Following the hydrothermal process of glucose, carbon nanorods retain their basic appearance with cylinder outlines.

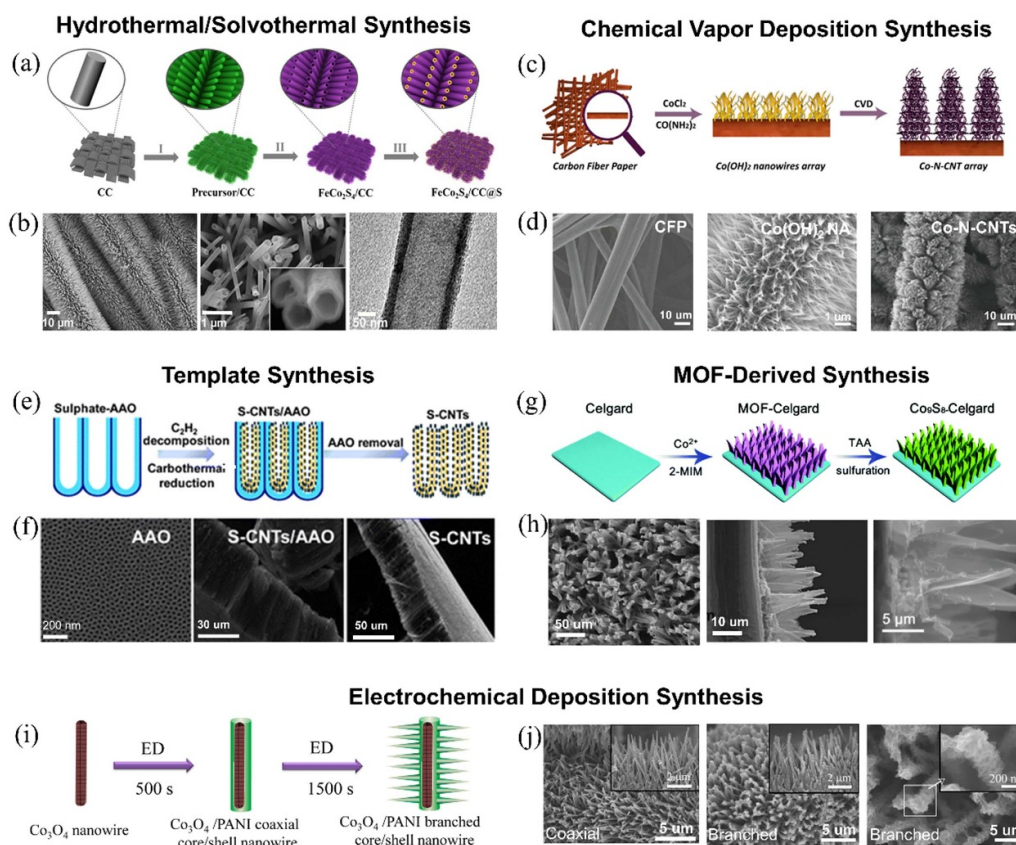


Figure 2. The widely used methods for the synthesis of NAs. (a) Schematic illustration of the hydrothermal synthesis process of FeCo_2S_4 nanotube arrays on carbon cloth. (b) Field-emission scanning electron microscopy (FESEM) and transmission electron microscopy (TEM) images of $\text{FeCo}_2\text{S}_4/\text{CC}$. Reprinted with permission from [60]. Copyright (2018) American Chemical Society. (c) Schematic illustration of the CVD synthesis process of a Co-N-CNTs array. (d) SEM images of CFP substrate, precursor $\text{Co}(\text{OH})_2$ nanowires array, and Co-N-CNTs array. Reprinted with permission from [65]. Copyright (2019) American Chemical Society. (e) Schematic illustration of the AAO template synthesis process of S-CNTs. (f) SEM images of AAO template, S-CNTs/AAO and S-CNTs. Reproduced from [73] with permission from the Royal Society of Chemistry. (g) Schematic illustration of the MOF-derived synthesis process of Co_9S_8 -Celgard. (h) SEM images of the top and side views of Co_9S_8 -Celgard. Reproduced from [80] with permission from the Royal Society of Chemistry. (i) Schematic illustration of the electrochemical deposition synthesis process of $\text{Co}_3\text{O}_4/\text{PANI}$ core/shell NAs. (j) SEM images of coaxial (after a shorter electrodeposition) and branched (after a longer electrodeposition) $\text{Co}_3\text{O}_4/\text{PANI}$ core/shell nanowire arrays. Reprinted with permission from [87]. Copyright (2013) American Chemical Society.

Owing to the use of different templates, this versatile approach achieves a feasible dimension controllability and uniformity of the architectural arrays. The template method offers several advantages over direct synthesis, including precise control over the shape and size of materials, as well as the ability to achieve high levels of uniformity and stability. However, the crystalline quality and purity control during template filling and removal are major points of difficulty in the template synthesis approach. Therefore, as a novel construction approach for the development of sustainable energy systems, this templating technique offers promising features with significant advantages and limitations.

3.4. Metal-organic framework (MOF)-derived synthesis

MOFs or porous coordination polymers, are a type of porous hybrid crystalline materials that are composed of

coordination bonds between the organic ligand and the transition metal cation [75, 76]. These hybrid materials have received broad attention because MOFs can be synthesized rationally with high porosity, large internal surface area, uniform and adjustable pore sizes [77]. MOF-derived synthesis has been used for the preparation of porous materials (e.g., oxides, chalcogenides, and phosphides) with advantages of low cost, simple setup, and flexible operations [54].

Multi-functional nano wall arrays (MNWAs) [78] with unrestricted Li ion transport channels were designed via a one-pot pyrolysis of Co-based MOF arrays with CNTs grown on the surface, which were applied as a cathode host for Li-S batteries. Wang *et al* designed a novel sulfur cathode incorporating sulfur, flexible carbon cloth, and N-doped carbon NAs derived from MOFs with embedded CoP ($\text{CC}@\text{CoP}/\text{C}$) [79]. In addition to the synthesis of MOF-based materials on carbon felt or carbon paper, some research has been done to synthesize Co_9S_8 materials directly on the separator to obtain excellent

electrochemical performance [80]. The well-aligned hollow Co_9S_8 nano wall arrays grown *in situ* on a separator were prepared and performed as an efficient polysulfides barrier for high performance Li–S batteries (figures 2(g) and (h)).

3.5. Electrochemical deposition synthesis

The process of electrochemical deposition synthesis involves the formation of a sedimentary layer on a solid surface through a redox reaction facilitated by an external power supply. The involvement of electrochemical deposition in versatile synthetic chemistry offers an alternative approach to the production of architectural arrays due to the advantages of safety, simplicity of requirements, low synthesis temperature and high accessibility, as well as making it easy to realize industrial manufacturing. In an electrodeposition process, NAs can be grown on the solid–liquid surface of an electrode through the migration of ions in the electrolyte under a certain voltage or current. The onset of electrodeposited materials is typically accompanied by the gain or loss of ions from the electrode, which can be used to grow the desired NAs of materials on the surface of the electrode [81, 82]. Electrodeposition allows NAs to be prepared in a short period of time. By varying the electrolyte composition, current density, reaction time, and other parameters, the composition and morphology of NAs can be well tuned [83, 84]. Therefore, the electrodeposition method can be used to fabricate various NAs including metal oxides and other metal compounds on conductive substrates, and it is also widely used for the growth of polymer NAs, where the morphology may be well controlled by deposition time [54, 85].

Elias *et al* reported a novel approach to fabricating well ordered hollow urchin-like single-crystal ZnO nanowires with controlled nanowire and core dimensions [86]. The ordered nanostructures result in strong light scattering properties, offering promising applications as building blocks for different types of nanostructured solar cells. High-quality NAs of metallic oxide/conducting polymer hetero-structures were also fabricated by the controllable electrochemical polymerization of conducting polymer shells on preformed metallic oxide nanostructures [87]. It is interesting to note that the morphology of the polyaniline (PANI) shell can be tuned from coaxial to branched shell by lengthening the electrodeposition time. As the deposition time increased to 1500 s, the surface roughness increased and PANI nanopikes of ~ 15 nm in average diameter were formed, resulting in a branched Co_3O_4 /PANI core/shell nanowire structure (figures 2(i) and (j)). Li *et al* demonstrated a simple electrochemical assembly strategy for realizing vertically aligned sulfur-graphene (S-G) nanowalls on electrically conductive substrates [88]. Remarkably, in each individual S-G nano wall, the sulfur nanoparticles were homogeneously anchored between the ordered graphene layers that were favorable for the diffusion of Li ions and transport of electrons.

In conclusion, a variety of synthesis schemes can be employed to fabricate nano array structures with regular morphology and sequence. However, each method possesses its own advantages and limitations, which are summarized in

table 1. When determining the appropriate synthesis route during the preparation process, it is essential to consider the experimental requirements and production objectives, striving to attain fine controllability, minimize energy consumption, and achieve cost-effectiveness.

4. Applications in Li–S batteries






4.1. Sulfur cathode

The sulfur cathode of Li–S batteries still faces the following critical issues: (i) the ‘shuttling effect’ arising from dissolved lithium polysulfides, (ii) the poor ionic/electrical conductivity of sulfur and Li_2S , and (iii) the large volumetric change during charge/discharge processes (up to 80%), which greatly hinders the practical application of Li–S batteries. In comparison to traditional slurry casting electrodes, the fabrication of sulfur cathodes in the form of NAs unfolds various outstanding properties such as binder-free, fast ion/electron transfer, high mechanical strength against volumetric changes, and high sulfur loading [89–91]. In the following subsections, some representative NAs for sulfur cathodes are presented and discussed in detail.

4.1.1. Nanostructured carbon arrays. Nanostructured carbon materials have been considered as valid hosts for sulfur due to their large specific surface area, high conductivity, natural abundance, and good mechanical strength [92–94]. A carbon matrix can effectively confine sulfur or soluble polysulfides, which significantly reduces the shuttling effect and enhances the electrochemical performance of sulfur cathodes. Of these, nanostructured carbon NAs with large void spaces not only allow uniform sulfur distribution for high sulfur loading, but also facilitate the electron/ion transport between the sulfur and the host to enable a high sulfur utilization ratio. The main types of nanostructured carbon arrays employed as sulfur hosts are: one-dimensional (1D) NAs (e.g. nanofibers and nanotubes), two-dimensional (2D) NAs (e.g. nanosheets and nanowalls), three-dimensional (3D) NAs (e.g. nanorods), and heteroatom-doped carbon arrays.

NAs of 1D carbon are favorable for electron transport and have a large surface area for the deposition of $\text{Li}_2\text{S}/\text{Li}_2\text{S}_2$. Cui and coworkers reported hollow carbon nanofiber arrays filled with molten sulfur as the sulfur electrode and achieved a high specific capacity of about 730 mA h g^{-1} at a 0.2 C rate after 150 cycles (figure 3(a)). In addition to effectively trapping sulfur species, the hollow structure with high aspect ratio can also cope with volume expansion [95]. However, despite the advantages of not requiring polymer binders and conductive additives, the limited space between the 1D NAs is detrimental to ion diffusion, leading to poor performance at high rates [96]. Thus, 2D materials also attract significant attention for Li–S batteries due to the advantages of great surface-to-mass ratio, high conductivity, and high mechanical strength. Piao *et al* synthesized honeycomb-like ordered mesoporous carbon nanosheet arrays (NSAs) with a large pore volume and a high surface area that exhibited excellent electrochemical

Table 1. Summary and comparison of different synthetic routes.

Synthesis methods	Schematic	Advantages	Disadvantages
Hydrothermal/solvothermal synthesis		Well controlled crystal structure and morphology; simple preparation process; simple equipment; environmentally friendly.	Longer reaction times; invisible reaction process.
Chemical vapor deposition		Can be well controlled; high working efficiency; high precision of the material.	Possible pollution; low utilization; high operating cost;
Template synthesis		Precise control; high uniformity and stability.	Templates are sacrificed and difficult to scale; single morphology and structure.
MOF-derived synthesis		Low cost; simple setup; flexible operations.	Limited type of materials.
Electrochemical deposition synthesis		Can be well controlled safety; simple equipment; low synthesis temperature; high accessibility.	Heterogeneous grain; aggregation of catalysts; limited to simple material preparation.

performance (figure 3(b)). The unique 2D porous array architecture can be used as an excellent sulfur host for homogeneous sulfur loading and polysulfides trapping, thereby improving sulfur utilization and retaining a stable cycling lifetime. After 500 cycles, the sulfur-loaded electrode showed a reversible capacity of $505.7 \text{ mA h g}^{-1}$ at 0.5 C, which was much higher than that of a sulfur cathode without a porous array structure (339 mA h g^{-1}) [97]. In comparison to 1D and 2D NAs, the free-standing 3D NAs could further improve the electron and ion transport and release mechanical stress during cycling. Moreover, the areal specific capacity and energy density can be enhanced by increasing the height of the 3D array electrodes and the amount of electrode material in a given area [98]. As shown in figure 3(c), Tu *et al* designed free-standing carbon–sulfur cathodes with 3D carbon nanorods arrays with a high mass loading of sulfur ($\sim 80.55\%$). Such a 3D NA structure can efficiently increase the specific surface area, provide abundant ion/electron transport paths and suppress the shuttling effect of polysulfides [74].

In addition, nanostructured carbon with heteroatom doping can substantially enhance the anchoring of polysulfides by chemical bonding, which will suppress their movement

and diffusion into the electrolyte [99–101]. Heteroatom doping has been implemented in a variety of carbon NAs. Sun *et al* fabricated MNWAs by pyrolysis of a Co-based MOF in combination with CNTs growth (figures 3(d)–(f)). Because of synergetic effects between the physical limitation of the vertically aligned channels and chemical interactions between metallic Co and polysulfides, the S/MNWA electrodes with 4 mg cm^{-2} sulfur loading showed good cycling stability with a 72% capacity retention after 400 cycles at a current density of 3.2 mA cm^{-2} . When the sulfur loading was increased to 10 mg cm^{-2} , the electrode was still able to deliver a high areal capacity of $12.4 \text{ mA h cm}^{-2}$ with a high capacity retention of nearly 85% over 100 cycles [78]. Our group proposed an entangled CNT array with N doping and encapsulated Co nanoparticles, which served as an effective host for a sulfur cathode (figures 3(g)–(i)). Doping of the polar N species promoted chemical adsorption with the polysulfides, and therefore limited their diffusion. Moreover, the encapsulated Co nanoparticles can efficiently catalyze the redox kinetics of sulfur species, thereby reducing the accumulation of soluble polysulfides and preventing the shuttling effect. With the effective anchoring and rapid conversion of polysulfides, the assembled

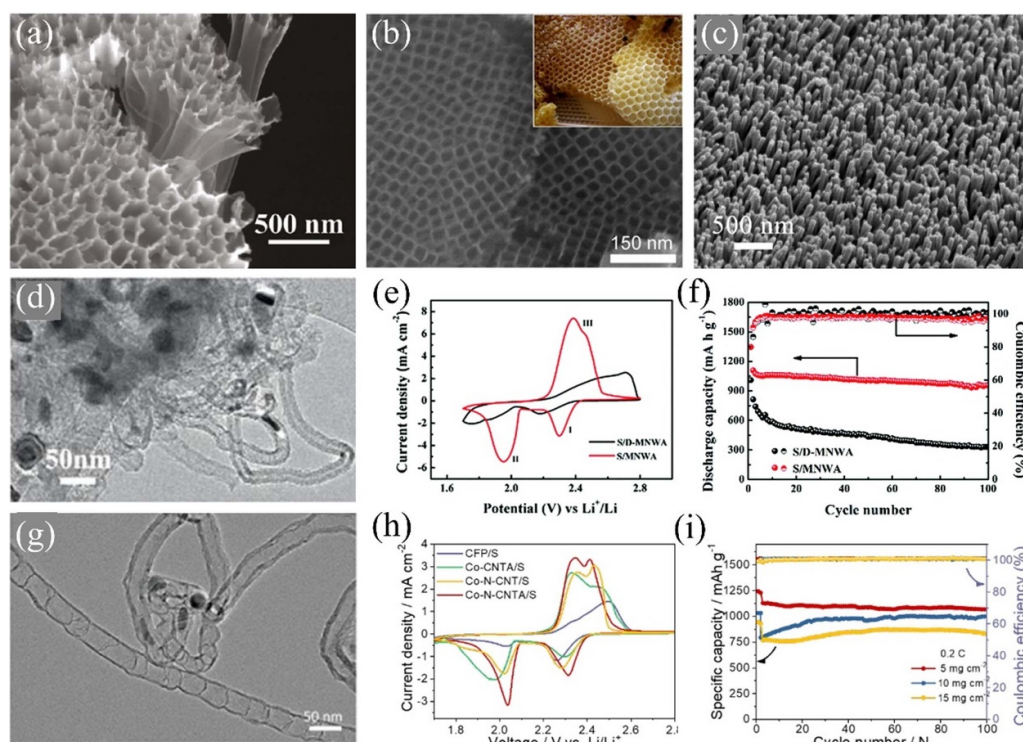


Figure 3. Nanostructured carbon arrays employed as sulfur hosts. (a) SEM image of a 1D hollow carbon nanofiber. Reprinted with permission from [95]. Copyright (2011) American Chemical Society. (b) SEM image of 2D ordered mesoporous carbon nanosheets. Reprinted with permission from [97]. Copyright (2017) American Chemical Society. (c) SEM image of 3D carbon nanorods. Reprinted from [74]. Copyright (2016), with permission from Elsevier. (d) TEM images of MNWAs. (e) CV profiles and (f) cycling stability at 1.3 mA cm^{-2} of S/MNWA and S/D-MNWA (the structure of MNWA is destroyed) electrodes. Reproduced from [78] with permission from the Royal Society of Chemistry. (g) TEM image of bamboo-like CNTs and Co-N-CNTs array. (h) CV curves and (i) cycling performance of Co-N-CNTA/S. Reprinted with permission from [65]. Copyright (2019) American Chemical Society.

Li-S batteries delivered a high capacity of 814 mA h g^{-1} after 1000 cycles at 1 C with a very low capacity decay rate of 0.014% per cycle. Owing to the superiority of the NAs structure, these benefits can even be extended to sulfur loading as high as 15 mg cm^{-2} . More importantly, the assembled pouch cells can exhibit a stable cycling for more than 150 cycles and readily turn on 80 light-emitting diodes overnight, demonstrating the feasibility of NA electrodes for practical applications [65].

The sulfur/carbon cathodes mentioned above were prepared by filling the pores with molten sulfur or sulfur-containing liquids [18, 102]. However, pores fully filled with sulfur chunks hinder rapid penetration of electrolyte and the fast transport of ions/electrons, which increases the cathode polarization and decreases sulfur utilization. To address this issue, Cheng *et al* prepared S-CNTs arrays by using a sulphate-containing AAO template, which confined sulfur within the nanotube walls. As a synthesized S-CNTs cathode consists only of elemental carbon and sulfur, the weight percentage of sulfur can reach 50%. Sulfur nanoparticles with a diameter of 1–10 nm were evenly located between the graphene layers, which restricted the mobility of sulfur species owing to physical confinement [73]. Yang's group demonstrated the synthesis of vertically aligned S-G nano wall arrays on electrically conductive substrates by the

electrochemical assembly of Na_2S -graphene oxide suspension during the cyclic voltammetry (CV) process. Sulfur nanoparticles are uniformly anchored between the vertical arranged graphene arrays on the substrate, which favors the rapid migration of both Li ions and electrons. In addition, the hierarchical and macroporous structure facilitates rapid electrolyte penetration and effective buffering of the volume fluctuation during repeated discharge/charge cycles. The electrode thickness can be tuned by adjusting the number of sweeps in the CV scanning. As the number of sweeps is increased to 20, the area specific mass density can be increased to 2.2 mg cm^{-2} [88].

4.1.2. Transition metal compound arrays. Transition metal compounds with intriguing nanostructures and electronic properties have been considered as effective sulfur hosts to replace the nonpolar carbon matrix [103, 104]. The polar surface of transition metal compounds are conducive to strong chemical interactions with polysulfides, and thus possess a strong ability to absorb and entrap polysulfides, which significantly suppresses the shuttling effect [105, 106]. They can mitigate the loss of sulfur species and improve sulfur utilization, which endows Li-S batteries with improved reversibility and a more stable cycle life [107]. In this section, arrays of transition metal compound used as host materials for Li-S

batteries are classified into several categories: transition metal oxide arrays, transition metal sulfide arrays, transition metal phosphide arrays, and transition metal nitrides arrays.

Among various catalytic materials, transition metal (i.e. Mn, Co, Ti, Fe, and Mo) oxides have emerged as promising candidates to accommodate sulfur and chemical anchor polysulfides in Li–S batteries [108–112]. Metal oxides contain the O^{2-} state of oxygen, which provides abundant polar active sites to absorb polysulfides and further promote the electrochemical performance of sulfur cathodes. Unfortunately, metal oxides generally suffer from poor electrical conductivity, which significantly impedes electron transport and, as a result, decreases the electrochemical performance. It is therefore a sensible approach to fabricate active transition metal oxides arrays on conductive substrates with high electric properties and excellent stability. For instance, MnO_2 , VO_2 and CuO are promising electrocatalysts due to their unique surface chemistry. In earlier studies, it was found that the polysulfides would be oxidized to insoluble thiosulfates on the surface of MnO_2 , VO_2 and CuO with redox potentials in the range of 2.4–3.05 V. Furthermore, thiosulfate serves as a mediator to catenate and bind more long-chain polysulfides, and reduces them to insoluble lithium sulfide [109, 113]. Sun *et al* synthesized a free-standing 3D hierarchical structure with paramonitroite VO_2 nanoparticles grown on parallel nitrogen-doped CNT arrays ($VO_2(P)\text{-NCNT}$) (figure 4(a)). Compared to the CV data of the NCNT/S cathode, $VO_2(P)\text{-NCNT/S}$ showed lower polarization and a shift in the onset potential of the reaction with improved redox kinetics (figures 4(b) and (c)). As a result, the $VO_2(P)\text{-NCNT/S}$ cathode delivered a stable long-term cycling with a capacity retention of $\sim 67\%$ after 500 cycles at 2.0 C, and a high areal loading of 9.6 mg cm^{-2} with an initial areal capacity of $10.2 \text{ mA h cm}^{-2}$ at 0.2 C for 200 cycles [114]. Unfortunately, the oxidation of polysulfides and formation of thiosulfate could not occur on metal oxides with low redox potentials. Instead, the catalytic activity of these metal oxides comes from the superior affinity of the polar surface toward polysulfides. For instance, a Co_3O_4 nanoneedle array grown on flexible carbon cloth ($CC@Co_3O_4$) has been reported as a catalytic host for high-performance sulfur cathode. The high affinity of Co_3O_4 for soluble polysulfides is favorable for polysulfides conversion during the discharge, and the electrocatalytic activity of Co_3O_4 accelerates the decomposition of Li_2S_2/Li_2S in the charging process. It should be noted that the nanoneedle array provides sufficient and homogeneous active sites for the continuous deposition of Li_2S_2/Li_2S . The $S/CC@Co_3O_4$ electrode thus exhibits a low capacity decay rate of 0.049% per cycle at 2.0 C for 500 cycles [115]. Zhang *et al* combined the advantages of NAs and closed structures to effectively adsorb polysulfides. The sulfur cathode based on a ‘room-like’ TiO_2 array structure showed both high sulfur utilization and a long cycle life [116]. Transition metal sulfides have also been proved to be efficient and stable catalysts for Li–S batteries [117–119]. There are many merits for using transition metal sulfides as catalysts in Li–S batteries:

- (i) Strong sulfiphilic property towards polysulfides.
- (ii) Higher electrical conductivity than metal oxides. Some metal sulfides even have metallic or semi-metallic properties.
- (iii) Low lithiation potential (below 1.5 V vs. Li^+/Li). This helps to avoid parasitic reactions due to overlap with the operating potential range in Li–S batteries [120].

The Co_9S_8 tubules array was reported as a sulfur host for Li–S batteries. Co_9S_8 entrapped lithium polysulfides for a long cycle life owing to its high conductivity and strong sulfiphilic affinity. As a result, the $S@Co_9S_8$ composite cathode maintained a high capacity of $756.6 \text{ mA h g}^{-1}$ after 600 cycles at a 1 C rate and a low capacity decay of 0.026% per cycle [61]. Additionally, $FeCo_2S_4$ nanotube arrays and $NiCo_2S_4$ nanoneedle arrays were also constructed as self-supported sulfur hosts for high loading Li–S batteries [60, 121]. More recently, defect engineering has been extensively studied in the design of sulfur hosts for Li–S batteries. Chen *et al* synthesized a sulfur-deficient ZnS nanotube array on carbon cloth ($ZnS_{1-x}\text{-CC}$) (figure 4(d)). ZnS_{1-x} arrays can provide abundant reaction active sites, enough buffer space for the volume change of sulfur and facilitated electrolyte infiltration. Furthermore, the electronic structure of ZnS was regulated by sulfur-vacancy engineering, thus facilitating polysulfides confinement and rapid sulfur reaction kinetics. A higher initial capacity and a lower capacity decay rate were observed on the $Li_2S_6/ZnS_{1-x}\text{-CC}$ electrode compared with $Li_2S_6/ZnS\text{-CC}$ and $Li_2S_6\text{-CC}$, further confirming that sulfur deficient sites adsorb polysulfides, thereby improving sulfur utilization and suppressing the shuttling effect (figures 4(e) and (f)) [122]. Furthermore, bimetallic sulfides with NAs structure have also been explored for sulfurs cathode. Chen *et al* proposed the preparation and application of bimetallic sulfide NSAs ($CoZn\text{-S}$), which regulated the electronic structure and promoted the electron transfer process through vacancy and interface modification. The amount of Li_2S deposition ($311.1 \text{ mA h g}^{-1}$) and peak current intensity of $CoZn\text{-S}$ were shown by nucleation experiments to be far superior to those of the monometal sulfide. The $CoZn\text{-S}$ cathode showed the best capacity retention under the same test conditions. The $CoZn\text{-S}$ cathode was then applied in a more realistic application with more rigorous parameters. Surprisingly, the cell can still run smoothly under the harsh conditions of high-sulfur-loading up to 9.2 mg cm^{-2} and a low E/S ratio of $3 \mu\text{l mg}^{-1}$ [123].

To date, a variety of transition metal phosphides have been adopted as catalysts for the redox reaction of polysulfides in Li–S batteries, such as CoP , FeP , Ni_2P , and MoP_2 [54, 124–126]. Zhu *et al* reported an MOF-derived CoP -embedded hollow carbon NSAs grown on carbon cloth ($CC@CoP/C$) (figure 4(g)). The embedded CoP nanoparticles synergize the anchoring and electrocatalysis of polysulfides, thereby improving the utilization of sulfur and facilitating redox kinetics. The $CC@CoP/C\text{-S}$ cathode exhibited a higher first discharge capacity and a more stable cycle life than the $CC@Co/C\text{-S}$ and $CC/C\text{-S}$ cathode, demonstrating NA

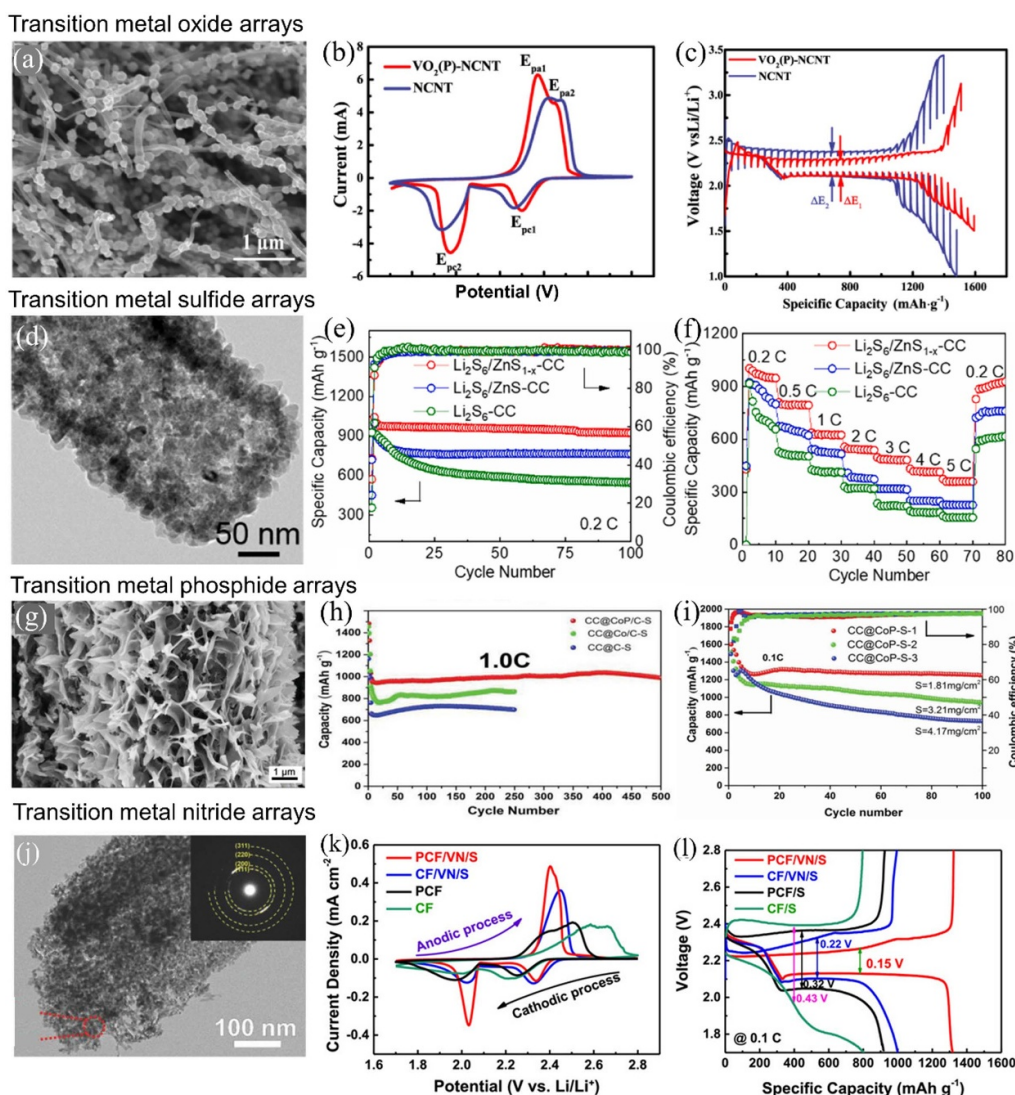


Figure 4. Transition metal compound arrays employed as sulfur hosts. (a) FESEM image of the $\text{VO}_2(\text{P})\text{-NCNT}$. (b) CV curves and (c) EIS curves of NCNT/S and $\text{VO}_2(\text{P})\text{-NCNT/S}$ cathodes. Reprinted from [114]. Copyright (2019), with permission from Elsevier. (d) TEM image of the ZnS_{1-x} nanotube. (e) 0.2 C cycle life and (f) rate-performance of the cells with $\text{Li}_2\text{S}_6/\text{ZnS}_{1-x}\text{-CC}$, $\text{Li}_2\text{S}_6/\text{ZnS-CC}$ and $\text{Li}_2\text{S}_6\text{-CC}$ electrodes. Reprinted from [122]. Copyright (2021), with permission from Elsevier. (g) SEM image and (h) long-term cycling performance of CC@CoP/C-S electrodes. (i) Cycling performance of CC@CoP/C-S cathodes with high sulfur loadings [79]. John Wiley & Sons. [© 2019 WILEY-VCH Verlag GmbH & Co. KGaA, Weinheim]. (j) TEM image of VN nanobelts (inset: the selected area electron diffraction (SAED) patterns of VN). (k) CV curves and (l) discharge/charge profiles of the cells with PCF/VN/S, CF/VN/S, PCF/S, and CF/S electrodes. [131] John Wiley & Sons. [© 2022 Wiley-VCH GmbH].

structure and phosphide catalysts are both vital for designing electrodes to maximize catalytic effects (figures 4(h) and (i)) [79]. Xiao *et al* proved the electrocatalytic effect of CoP/NC is higher than $\text{Co}_9\text{S}_8/\text{NC}$ through comparison of the CV curves of a symmetric cell with a Li_2S_6 catholyte and theoretical calculation [127]. Zhu *et al* conducted a systematic investigation of the electrochemical performance of sulfur in oxide-based and phosphide-based hosts. It was found that S/CF/FeP@C (carbon cloth with grown FeP@C nanotube arrays) cathode showed much better performance than that of the S/CF/Fe₃O₄@C cathode. The first-principles calculation has revealed that P atoms are more likely to bind with or separate from other atoms, and the bonding and breaking of S–P is easier than S–O, leading to fast electron transfer and fast

polysulfides transformation dynamics. Therefore, the position of the p-band originating from the P-anion is particularly efficient in propelling sulfur conversion [128].

In addition, transition metal nitrides have also attracted widespread attention due to their unique electronic structure, high electronic conductivity and desirable structural stability [129]. For example, Zha *et al* demonstrated that 3D titanium nitride nanowire arrays with highly exposed (200) facets with five-coordinated Ti active sites have a strong ability for chemically anchoring polysulfides, thus limiting the shuttling effect [130]. Moreover, Tu and co-workers compared the electrochemical performances of sulfur cathodes with or without vanadium nitride (VN) on porous carbon fiber (PCF) arrays (figure 4(j)). The sulfur cathode

with PCFs/VN arrays exhibits superior performance to others (figures 4(k) and (l)). Of these, PCF with high surface area and large porosity enables high sulfur loading and physically constrains polysulfides diffusion; meanwhile, the embedded VN with strong chemical activity effectively suppresses the shuttling effect of polysulfides. Notably, these benefits can be extended to the cathode with a high sulfur loading of 8.1 mg cm^{-2} [131]. Zhan *et al* further embedded Co nanoparticles in self-supported porous VN arrays coupled with N-doped CNTs (CC/VN/Co@NCNTs/S). With the combination of the highly conductive VN, Co nanoparticles and NCNT, the electron transport and catalytic sulfur conversion were significantly improved. The CC/VN/Co@NCNTs/S cathode showed a high reversible capacity, excellent rate performance ($625.3 \text{ mA h g}^{-1}$ at 5 C) and long cycle stability with a low capacity decay rate of 0.063% per cycle at 1 C for 500 cycles [132]. Shen *et al* fabricated a 2D N-doped carbon array with Co_4N particles derived from MOFs on carbon cloth. The Co_4N nanoparticles improved the rate performance of the sulfur cathode by decreasing the polarization of the electrode to accelerate the sulfur conversion reactions [133]. In addition to the common transition metal compounds mentioned above, there is some research dedicated to the design and preparation of transition metal carbides (MoC [134–136], B_4C [137]), transition metal selenides (NiSe_2 [138], CoSe_2 , etc) for sulfur cathodes.

In short, these NAs structures exhibit good conductivity, porous structure, and rich catalytic active sites, which can effectively entrap soluble polysulfides and propel the sulfur conversion reaction, thus significantly improving the capacity, rate performance, and cycling stability of the sulfur cathode. From a more attractive perspective, analysis and calculation of the catalytic conversion of sulfur species at the atomic level will provide insights into the design of host materials for sulfur cathodes with excellent electrochemical performance.

4.1.3. Heterostructure arrays. Heterostructure engineering is one of the most promising approaches for achieving multiple functions with individual components. The beneficial synergistic effect results from the rational selection and integration of multiple elements into heterostructures, combining the advantages of various materials to balance the drawbacks of each component [139, 140]. Therefore, heterostructure arrays provide a general strategy to achieve more stable long-term cycling performance in Li–S batteries at high sulfur loading.

Generally, metal oxides manifest considerable chemical adsorption for the polysulfides due to their high polarities. However, sluggish surface diffusion and low electrical conductivity indicate inactive reaction kinetics, thereby reducing the sulfur utilization. Meanwhile, MXenes possess excellent carrier mobility, electrical conductivity, and strong adsorption capacity for the polysulfides. As a result, Zhu and colleagues created a 3D grid heterostructure with $\text{VO}_2(\text{p})$ nanorod arrays grown on the surface of 2D V_2C nanosheets (figure 5(a)). Along with V_2C , $\text{VO}_2(\text{p})$ nanorod arrays can increase electrode conductivity, enhance polysulfide adsorption, and catalyze the conversion of long-chain polysulfides to short-chain,

which dramatically reduces the shuttling effect and speeds up electrode reaction kinetics. In the meantime, a vertically grown $\text{VO}_2(\text{p})$ nanorod array improved the electron conductivity and provided spatial support for the V_2C nanosheets and supplied widely dispersed active sites for the continuous deposition of $\text{Li}_2\text{S}_2/\text{Li}_2\text{S}$. The $\text{VO}_2(\text{p})$ – V_2C heterostructure showed higher initial capacity (1250 mA h g^{-1} at 0.2 C), longer cycle life (500 cycles with 69.1% retention at 2 C) and high sulfur loading (10.2 mg cm^{-2}) (figures 5(b) and (c)) [141]. Yang and coworkers proposed a synergistic engineering strategy, which combines core–shell heterostructure with oxygen vacancies (OVs) in a free-standing 2D nanosheets array (figure 5(d)). The porous core–shell Co@CoO_{1-x} nanosheets array grown on carbon cloth was prepared as a high-performance catalytic host for sulfur cathodes (figures 5(e) and (f)). The abundance of OVs enhanced the electrical conductivity of CoO_{1-x} shells which manifest strong chemical interaction with polysulfides to facilitate the breakdown of the S–S bond. Additionally, the porous structure provided CoO_{1-x} shells with a large number of exposed active sites to produce powerful polysulfides adsorption capacity. Thus strategies to increase the intrinsic conductivity of metal oxides by creating OVs and doping with other transition metals may be promising [142].

Metal sulfide, and metal nitride heterostructures have attracted great attention, owing to their high electrical conductivity and rapid surface reactions. Sun's group designed a MoS_2 – MoN heterostructure nanosheets grown on CNT arrays as a 3D free-standing cathode. The high-resolution transmission electron microscopy (HRTEM) results show the close-fitting and atomically matched interfacial contact between MoS_2 and MoN (figure 5(g)). In this heterostructure, MoN provides coupled electrons to accelerate the redox polysulfide reaction, while MoS_2 , with a 2D layered structure, provides moderate polysulfides trapping ability and fast surface Li ion diffusion. Compared with a single component, MoN and MoS_2 could mutually boost the process of the 'adsorption-diffusion-conversion' of polysulfides, which has a synergetic enhancement effect to restrain the shuttling effect. As a result, the designed heterostructure cathodes exhibit a high rate capability up to 6 C and a low electrolyte volume/sulfur (E/S) ratio of 6.3 ml g^{-1} (figures 5(h) and (i)) [66]. Qiu *et al* designed a new type of P–N heterostructure embedded into carbon hollow NSAs grown on carbon cloth. An HRTEM image further confirms a clear hetero-interface formation between Co_4N and Co_9S_8 (figure 5(j)). The electrochemical performance of dramatic catalysts; $\text{CC@Co}_9\text{S}_8$ – Co_4N , $\text{CC@Co}_9\text{S}_8$, $\text{CC@Co}_4\text{N}$, and CC electrodes were investigated (figures 5(k) and (l)). The heterostructures provide abundant active sites and boundary defects, enhancing the nucleation/conversion redox kinetics of Li_2S . Subsequently, electrodes with Co_9S_8 – Co_4N exhibited a more stable cycle lifetime and higher capacities [143].

To enhance the conductivity, adsorption, and catalytic properties of cathode materials towards the LiPSs redox process, several methods can be employed, including the incorporation of carbon materials, metal doping, transition metal-based compounds, and other approaches. In table 2, we provide a comprehensive summary of their advantages, disadvantages, and synthesis methods. This table aims

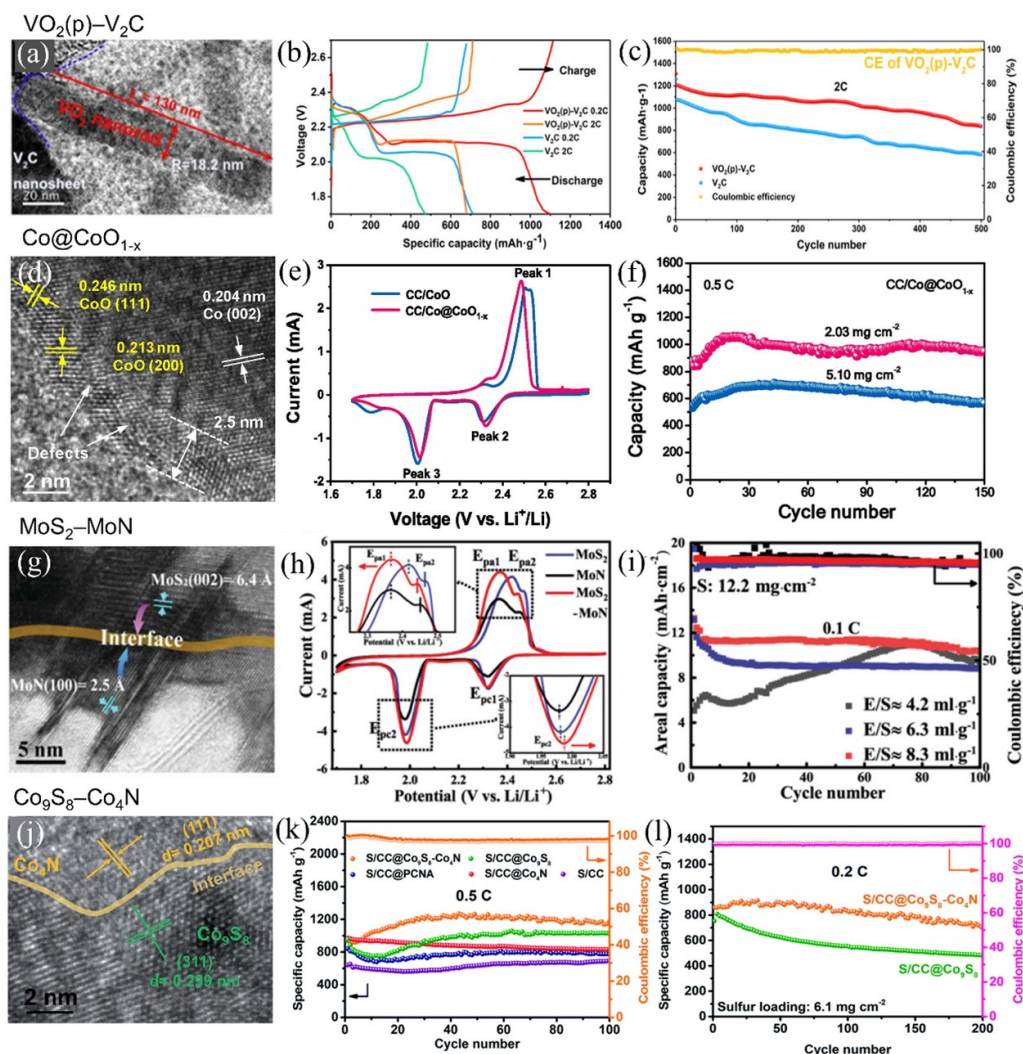


Figure 5. Heterostructure arrays employed as sulfur hosts. (a) TEM image of $\text{VO}_2(\text{p})\text{-V}_2\text{C}$. (b) Charge-discharge profiles and (c) long-term cycling performance of $\text{V}_2\text{C}/\text{S}$ and $\text{VO}_2(\text{p})\text{-V}_2\text{C}/\text{S}$ cathodes. Reprinted with permission from [141]. Copyright (2019) American Chemical Society. (d) HRTEM image of the $\text{CC}/\text{Co}@/\text{CoO}_{1-x}$. (e) CV curves and (f) cycling performances of $\text{CC}/\text{Co}@/\text{CoO}_{1-x}$. Reprinted from [142]. Copyright (2021), with permission from Elsevier. (g) HRTEM image of $\text{MoS}_2\text{-MoN}$ host. (h) CV curves and cycling performances of $\text{MoS}_2\text{-MoN}/\text{S}$ cathodes [66] John Wiley & Sons. [© 2021 Wiley-VCH GmbH]. (j) HRTEM image of the $\text{CC}@/\text{Co}_9\text{S}_8\text{-Co}_4\text{N}$ hollow nanosheet. (k) Cycling performance of the S/CC , $\text{S}/\text{CC}@/\text{Co}_4\text{N}$, $\text{S}/\text{CC}@/\text{PCNA}$, $\text{S}/\text{CC}@/\text{Co}_9\text{S}_8$, and $\text{S}/\text{CC}@/\text{Co}_9\text{S}_8\text{-Co}_4\text{N}$ electrodes. (l) Cycling performance of the $\text{S}/\text{CC}@/\text{Co}_9\text{S}_8\text{-Co}_4\text{N}$ and $\text{S}/\text{CC}@/\text{Co}_9\text{S}_8$ with high sulfur loading. Reproduced from [143] with permission from the Royal Society of Chemistry.

to assist researchers in selecting suitable NA materials for Li-S batteries.

4.2. Separator

A typical Li-S battery configuration consists of a sulfur cathode, and a lithium anode physically separated by the porous separator containing saturated electrolyte. As an integral part of Li-S batteries, separators act as electronic insulator and intrinsic ionic conductor. They separate the cathode and anode and prevent the battery from short-circuiting [66]. Separators mainly block the trans-membrane transport of polysulfides by adsorption, shielding and sieving, thereby suppressing the shuttling effect and battery self-discharge. On the other hand,

an increased mechanical strength of the separator can effectively prevent dendrite penetration during the electrochemical process, and enhance overall safety of the battery [144]. Currently, ‘expanded polypropylene (PP)’ is widely used as a separator and has been selected for commercial purposes, due to its low cost, excellent mechanical and electrochemical stability, high porosity, and good wettability for electrolyte and ion conductivity with micron-sized pores. However, as mentioned in many articles, during the charging and discharging process of Li-S batteries, polysulfides shuttle between the electrodes, and form insoluble Li_2S and Li_2S_2 layers on the lithium surface. This phenomenon inevitably triggers the wild growth and penetration of Li dendrites into the separator, which may lead to exothermic reactions between the

Table 2. Summary and comparison of different nanoarray materials.

Nanoarray materials		Strengths	Limitations	Synthesis method
Structural aspects	1D	High mass loading and the specific surface area.	Structural instability; limited space; poor conductivity.	Template-assisted; ALD; CVD.
	2D	Larger specific surface area; more electroactive sites; shortened pathways.	Restacking and aggregation of materials; the hindered transportation of electrolyte ions.	Template-free method; hydrothermal method; CVD
	3D	Excellent conductivity and large surface area; more flexible pore structure distribution.	Unfavorable volumetric energy density.	Template-free method; CVD
Transition metal compound arrays	Oxides	Strong polarity and shows high binding energies with LiPSs.	Weak conductivity and semiconducting; poor electron and ion transport.	CVD
	Sulfide	High electrical conductivity; strong LiPSs adsorbability and stability; auspicious electronic properties.	Lower conductivity compared to the carbonaceous materials.	Hydrothermal synthesis; MOF-derived; CVD
	Phosphides	Moderate adsorption to LiPSs and conductivity.	Easy to oxidize in air; complex synthesis; uncontrollable phase structures.	MOF-derived; CVD
	Nitride	Strong adsorption energy for LiPSs; higher conductivity; remarkable catalytic properties.	Agglomeration when present in high loadings.	CVD
	Hetero-structures	Coexistence of both adsorption and catalysis synergistically.	Complex preparation process; difficulty in obtaining uniform heterojunction structure.	CVD; MOF-derived; hydrothermal synthesis

organic electrolyte and electrodes that can result in a series of the internal short circuits and corresponding safety issues [145–147]. Therefore, it is essential to design novel composite separators that can adsorb soluble polysulfides or catalyze their conversion.

Separators using functional materials have been confirmed to be ion-selective, which is more promising for building a physical barrier to suppress the shuttling effect [107]. Most reviews discuss modified separators with different bands of coating material. Various modification methods and material structures exist for separator modification, including metals, transition metal-based compounds, MOFs, heterostructures etc [118, 144, 148]. Based on the structural design of several sulfur cathode materials, the advantages of NAs structure modified separator materials are highlighted due to their flexible nature. This chapter mainly deals with the modified

design of membrane materials, focusing on the introduction of NAs structures.

To resolve the severe dissolution of polysulfides and the lethal shuttling effect of the sulfur cathode, Chen *et al* used the MOF-derived hollow Co₉S₈ nano wall arrays grown *in situ* on a Celgard separator (Co₉S₈-Celgard) as an efficient polysulfides barrier for high-performance Li–S cells (figures 6(a) and (b)) [80]. Due to its well-designed structure, *in situ* growth/transformation, the polarity and high conductivity of Co₉S₈, Li–S batteries with the Co₉S₈-Celgard separator not only effectively blocked the polysulfides even with pure sulfur cathodes with a very high sulfur loading (5.6 mg cm^{−2}), but also delivered excellent specific capacity and outstanding rate performance. It showed a discharge capacity of 428 mA h g^{−1} at a high cycling rate of 2 C, while it recovered to 1270 mA h g^{−1} at 0.1 C (figures 6(c) and (d)). It is

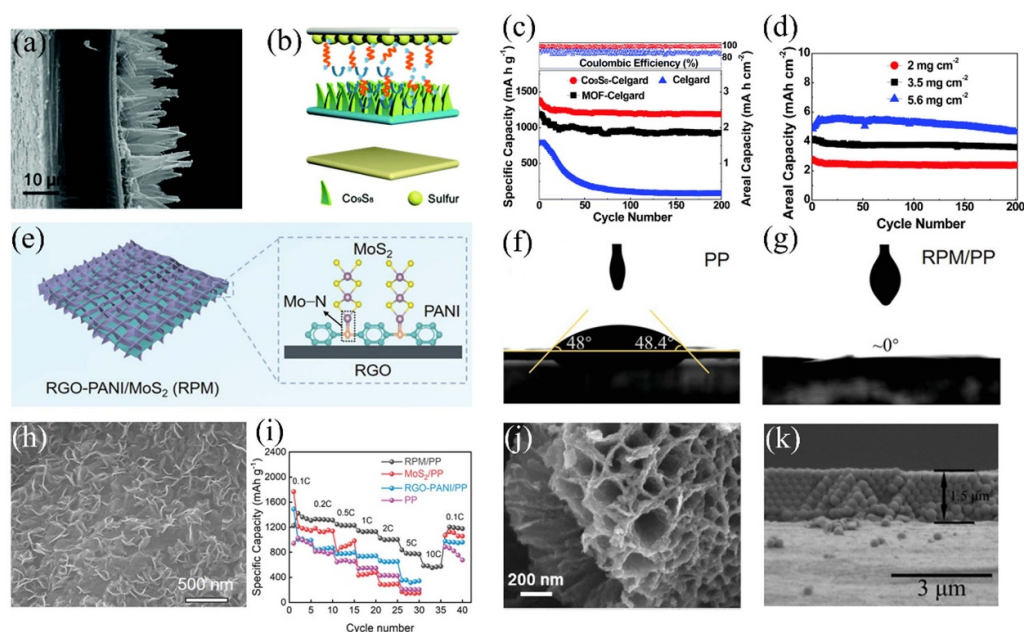


Figure 6. NA structures employed as separators. (a) SEM image and (b) the improvement mechanism of the Co_9S_8 -Celgard separator. (c)–(d) Cycling performance of Li–S cells with Co_9S_8 -Celgard separators. Reproduced from [80] with permission from the Royal Society of Chemistry. (e) Schematic illustration of the fabrication of RPM. (f)–(g) Contact angles between the electrolyte and pristine PP and RPM/PP separators. (h) SEM image of RPM. (i) Rate performance of Li–S cells with RPM/PP separators. [151] John Wiley & Sons. [© 2022 Wiley-VCH GmbH]. (j) SEM image of MPC separator. Reprinted from [152]. Copyright (2022), with permission from Elsevier. (k) SEM image of the PP/PMMA separator. Reprinted with permission from [153]. Copyright (2019) American Chemical Society.

the regular hollow array structure that effectively suppresses the shuttling effect, gives an excellent material stability, and improves the utilization rate of the active material sulfur.

Good separator wettability is crucial for a rapid ionic transport in Li–S batteries [149]. Jin *et al* improved wettability of the separator by modifying the surface of an ultrathin coating composed of polar NiOOH nano wall arrays and non-polar CNT conductive networks [150]. The lower contact angle compared with the PP meant that electrolyte could easily penetrate this composite separator which is beneficial for rapid ionic transportation. Shi *et al* obtained a Mott–Schottky heterogeneous layer modified separator through the vertical growth of MoS_2 arrays on the PANI *in situ* reduced graphene oxide (RGO) (figure 6(e)) [151]. The wettability of the separator to the electrolyte was investigated by contact angle measurements, and the RGO-PANI/ MoS_2 (RPM) separator displayed the most favorable surface wetting, which was beneficial for the infiltration of electrolyte and the diffusion of Li ion (figures 6(f) and (g)). The unique ‘reservoir’ structure developed by MoS_2 arrays and RGO-PANI substrate can effectively trap polysulfides, giving the cells excellent rate performance (553 mA h g^{-1} at 10 C) and outstanding cycle stability (524 mA h g^{-1} after 700 cycles at 5 C) (figures 6(h) and (i)). Kong *et al* prepared a hierarchical porous phosphorus doped carbon NSA as separator coating layer to realize an effective trapping-conversion of polysulfides (figure 6(j)) [152]. An array of nanoparticles on the surface of the PP separator is also considered as a good strategy. Deng *et al* designed an arrayed poly(methyl methacrylate) (PMMA) microspheres retarding layer coated on PP layer as the separator (figure 6(k)) [153].

The synthesized PMMA microspheres not only suppress the diffusion of polysulfides but also improve the affinity of the separator to the electrolyte.

Moreover, the NA structures achieve binder-free interference with *in situ* growth and infiltration percolating electron pathways. The modified membrane prepared by *in situ* one sided growth of polar CoSO_4 hydrate (CS/PP-6) has a needle-like array structure, and the large pore volume and specific surface area result in more catalytic activity [59]. Using the same growth method, Yang *et al* fabricated multifunctional NiCo_2S_4 (NiCoS) NSAs on a PP for high performance Li–S batteries [154]. The NiCoS NSAs were interconnected, conductive and closely adhered to the PP membrane without using any binder. Even at high sulfur loading of up to 5.3 mg cm^{-2} , the cell still approached a high reversible capacity of 495 mA h g^{-1} after 200 cycles.

4.3. Lithium metal anode

Li metal has become an ideal anode material due to its extremely high theoretical specific capacity (3860 mA h g^{-1}) and lowest reduction potential (-0.304 V vs. SHE) [42]. In a typical Li–S battery with a composite S/C cathode, Li is highly reactive and can react with most electrolytes to form a heterogeneous SEI. Subsequently, active polysulfides and fresh Li are consumed by side reactions, reducing coulomb efficiency (CE) and further diminishing the capacity of Li–S batteries. For this reason, researchers have proposed solutions in terms of ion distribution, deposition behavior etc., which are mainly divided into the following three

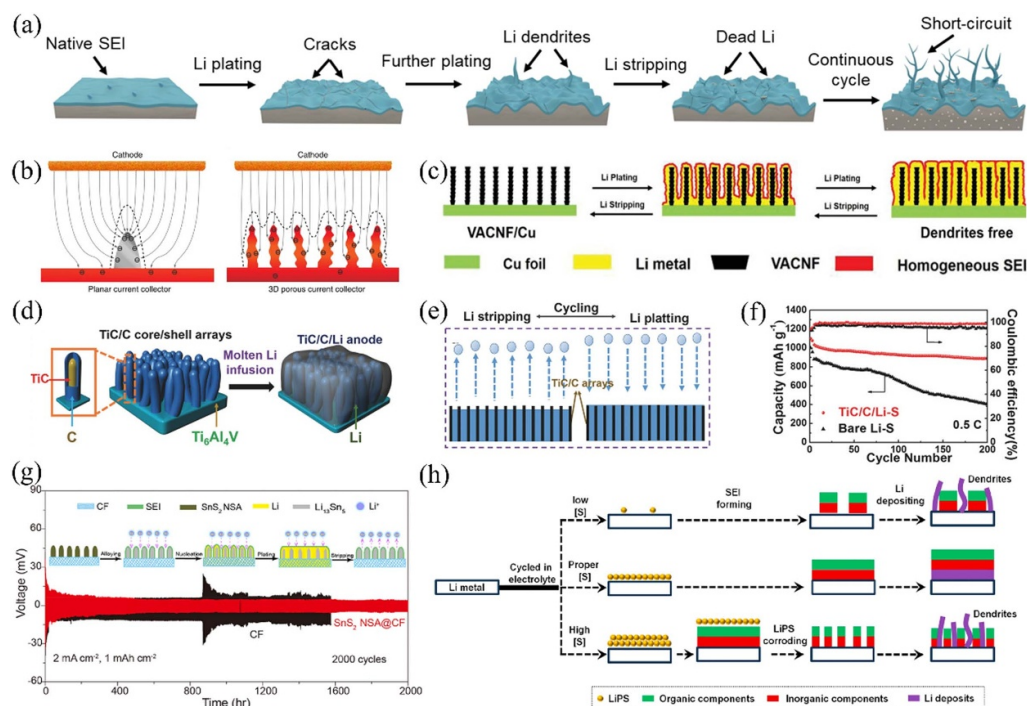


Figure 7. NA structures employed as Li metal anode. (a) Illustrated schematic of the failure process of a lithium anode. Reprinted with permission from [159]. Copyright (2022) American Chemical Society. (b) Schematic illustration of the proposed electrochemical deposition processes of Li metal. Reproduced from [160]. CC BY 4.0. (c) Schematic illustration of Li stripping/plating behavior of 3D VACNF/Cu host. [163] John Wiley & Sons. [© 2019 WILEY-VCH Verlag GmbH & Co. KGaA, Weinheim]. (d) Schematic illustration of the synthesis process of the TiC/C/Li anode. (e) Schematic illustration of the Li stripping/plating behavior of the TiC/C/Li electrode. (f) Cycling performance of Li-S cells with TiC/C/Li anodes. [48] John Wiley & Sons. [© 2017 WILEY-VCH Verlag GmbH & Co. KGaA, Weinheim]. (g) Schematic illustration of the Li nucleation and growth behavior on the SnS₂ NSA@CF. Voltage-time profiles of the symmetrical cells using Li@SnS₂ NSA@CF anode. Reprinted from [165]. Copyright (2021), with permission from Elsevier. (h) Schematic illustration depicting the influence of polysulfide concentrations on SEI evolution and Li deposition. Reprinted from [166]. Copyright (2016), with permission from Elsevier.

types: (a) surface protection - a protective film with excellent mechanical properties is constructed on the surface of the lithium metal anode to prevent dendrites from piercing; (b) lithium-carrying framework - using nano-materials with regular morphology as the 'host' for metal lithium deposition to reduce the volume change on the negative electrode side; (c) solid electrolyte - this type of the electrolyte can effectively prevent dendrites from penetrating and has extremely high safety [155–158]. Relatively low electrical conductivity is desirable when choosing an appropriate scaffold/framework material to prevent direct Li deposition. Given the vast toolbox of the expanding field of 2D materials and nanostructure synthesis, more scaffold designs are expected. This section mainly analyzes the causes of Li dendrites, introduces and summarizes the use of NAs structure for skeleton modification and subsequently optimizes the application advantages of the array structures.

Some studies have revealed the growth process of Li dendrites (figure 7(a)). Firstly, Li metal easily reacts with the electrolyte because of its high reactivity, resulting in the formation of an uneven SEI coating with unevenly distributed 'hot spots' on the surface. Large deposits are created under the SEI as a result of the uneven Li deposition and increasing inhomogeneity with cycles [159]. As a result of the SEI layer

breaking, numerous irregular cracks appear on the surface of the Li metal, causing severe Li dendritic formation. The dead lithium originates from the broken dendrite, and the freshly exposed lithium surface is corroded quickly by the electrolyte. Additionally, SEI with poor electronic conductivity forms surrounding broken Li, which ultimately results in electrode volume changes and major safety issues.

To resolve the problem, ideal anode structures must feature uniform surface curvature to equalize the electric field, and must be able to accommodate significant volume variation during cycling. Wang *et al* used 3D wood-derived carbon decorated with Ag, ZnO, and Au particles with a gradient distribution to create lithiophilic sites. This material exhibits exceptional 3D spatial controllability and gradient distribution of silver nanoparticles, which effectively enhances the uniform deposition of lithium. The average CE achieved at 1 mA cm⁻² is 99.8%, indicating excellent performance even under high current density conditions [61]. Yang *et al* demonstrated that a 3D current collector with a submicron-sized skeleton and NA structure can effectively improve the electrochemical deposition behavior of Li [160]. As shown in figure 7(b), many prominent peaks arranged on the submicron skeleton of the 3D Cu foil function as the charge centers and nucleation sites. This makes the electric field uniform, resulting in a uniform charge

distribution along the 3D skeleton. Consequently, Li nucleates and grows on the 3D current collector in nanosized chunks, filling the gaps of the arrays, and eventually forming a uniform Li surface. Luo *et al* designed an interconnected $\text{Li}_3\text{P}@ \text{Cu}$ mix ion/electron conductive interlayer (MCI) to address the issue of Li dendrites [161]. The *in-situ* generated Cu nanodomains provided abundant active sites for fast distribution of local current density, effectively lowering the energy barrier for Li nucleation. On the other hand, Li dendrites can also be suppressed by using a lithium plating method other than forming a framework structure on a lithium foil by an *in-situ* growth method. Xu *et al* synthesized a multifunctional lithium-pinned array endowed with functions of lithiophilicity, zoning effect and riveting effect on a surface phosphorized 3D copper foam [162]. Li can be uniformly plated/stripped both on the surface and in the inner space of the 3D skeleton with improved morphology. Cheng and coworkers designed a vertically aligned carbon nanofiber (VACNF) array with a unique and conically stacked graphitic structure directly grown on a planar Cu current collector (figure 7(c)). When used as a high-porosity 3D host with Li metal anodes, the Li–S batteries exhibited excellent rate capability and high cycling stability with no capacity fading over 600 cycles [163]. Liu *et al* described self-supported TiC/C core/shell nanowire arrays with diameters of 400–500 nm and confined hosts of molten Li forming an integrated trilayer TiC/C/Li anode (figures 7(d) and (e)) [48]. The as-prepared TiC/C/Li anode exhibited excellent electrochemical performance with a small hysteresis of less than 85 mV beyond 200 cycles (3.0 mA cm^{-2}) along with a very high CE up to 98.5% for 100 cycles at 1.0 mA cm^{-2} . More importantly, when the structured anode was coupled with a sulfur cathode, the assembled full cells separately displayed enhanced capacity retention and improved CE (figure 7(f)).

In addition, the lithiophilic character and poor spatial regulation can be challenging for Li nucleation/skeletal growth. Lithiophilicity and wettability of the protective layer materials have also emerged as the critical factors that researchers need to consider. Yang and coworker prepared a thin lithiophilic layer consisting of vertically aligned CuO nanosheets directly grown on a planar Cu current collector. The lithiophilic nature of the CuO nanosheets reduced the polarization of electrodes, ensuring uniform Li nucleation and a continuous smooth Li plating [164]. The vertical-aligned SnS_2 NSAs with intrinsic lithiophilic nature were uniformly decorated on highly flexible carbon foam ($\text{SnS}_2 \text{ NSA}@ \text{CF}$). $\text{Li}_{13}\text{Sn}_5$ formed *in-situ* uniformly induces Li nucleation on NSAs via a reduced Li nucleation overpotential [165]. Even after 100 cycles, the R_f of $\text{SnS}_2 \text{ NSA}@ \text{CF}$ values remained stable with a negligible fluctuation, indicating lithiophilic $\text{SnS}_2 \text{ NSA}$ effectively facilitates uniform nucleation and deposition of Li metal and thus maintained a stable SEI film (figure 7(g)).

Li–S batteries, require more sulfur loading and long-cycle stability for commercial applications. However, Li–S batteries with high sulfur areal loads typically have very short and poor cycling life. A battery with superior electrochemical performance requires interaction between cathode and anode

materials. A proper analysis of the effects of different sulfur loading on the SEI is necessary to obtain optimal application conditions. Yan *et al* proposed the role of polysulfides concentration on SEI evolution and Li deposition [166]. As shown in figure 7(h), when the polysulfides concentration is very low ($[\text{S}] < 0.05 \text{ M}$), the formation of a uniform SEI layer may hardly occur. The SEI prefers to be stable at a very high amount of electrolyte and a relatively low polysulfides concentration (0.10 M). When the sulfur concentration is very high ($[\text{S}] > 0.50 \text{ M}$) in the ether electrolyte, the cell exhibits a severe decay in efficiency even under the protection of 5.0 wt% LiNO_3 . Consequently, the sulfur content of the electrolyte on the anode should be reduced to around 0.10 M for Li–S cells with very high sulfur loading in order to exhibit a good cycle life.

5. Challenges of rational design for NA electrodes

Although significant process has been achieved in the research of NAs in Li–S batteries, there are still many obstacles to overcome. Arumugam *et al* introduced the concept of the ‘five 5 s’, which outlines five critical metrics essential for high-energy-density Li–S batteries, including sulfur loading $> 5 \text{ mg cm}^{-2}$, carbon content $< 5\%$, electrolyte-to-sulfur (E/S) ratio $< 5 \text{ ml mg}^{-1}$, electrolyte-to-capacity (E/C) ratio $< 5 \text{ ml (mA h)}^{-1}$, and negative-to-positive (N/P) ratio < 5 [167]. Meanwhile, the weight and volume of electrode material, as well as current collectors, should be lower possibly to achieve a higher energy density [168, 169]. Table 3 summarizes the reported NAs as electrodes for Li–S batteries. As displayed in figure 8(a) and table 4, due to the inherent advantages, most of the NA structure electrodes can achieve high sulfur loading, 44.2% of them can even realize a sulfur loading higher than 6 mg cm^{-2} . However, to obtain superior/maximum specific capacity, high sulfur loading and high sulfur utilization are key factors. Unfortunately, the electrolyte/sulfur (E/S) ratio has not received much attention. Although, lots of effort has been made toward achieving prolonged cycling performance, which is based on excessive electrolyte, the energy density is not up to the commercial standard even though sulfur loading is satisfactory along with excess electrolyte. As shown in figure 8(b) and table 5, 45.5% of the NA structure electrodes have an E/S ratio lower than $10 \mu\text{l mg}^{-1}$, while only 18.2% have a ratio lower than $5 \mu\text{l mg}^{-1}$. Most of the NA electrodes need to be wetted with a large amount of electrolyte to form the ion channels. It is a vital challenge to provide transfer channels for both ions and electrons in NA electrodes. Therefore, rational control of the E/S ratio needs to be taken seriously in order to achieve outstanding electrochemical performance and energy density.

Moreover, the relationship between the amount of electrolyte and sulfur utilization can be characterized by the electrolyte/capacity (E/C) ratio. This ratio is defined as the amount of electrolyte utilized per unit of discharge capacity in a cell. The E/C ratio is a direct reflection of the sulfur utilization in the

Table 3. Summary of nanoarray structures for the Li–S cells.

Classification	Cathode	Substrate	Sulfur loading (mg cm ⁻²)	Initial capacity (mA h g ⁻¹)	C rates /cycles	Capacity decay rate (%)	Sulfur loading (mg cm ⁻²)	E/S ratio (μl mg ⁻¹)	References
Nanostructured carbon arrays	Nanofibers/S	Al	1	~1400	0.2 C/150		1		[95]
	CNT/S	Freestanding	2–3	~950	1.5 A g ⁻¹ /100		3		[73]
	Graphene nanowalls/S	Cu/Ni sheet	1.3–2.2	1220	0.125 C/120		2.2		[88]
	OMC nanosheets/S		1–1.2	~700	0.5 C/500	~0.06	1.2		[97]
	CNAs/S	NF	2	1052	0.2 C/200	0.078	2	7.5	[74]
Heteroatom-doping	CNTs/S	CC	1.7	~900	0.5 C/300	0.1	1.7	24	[34]
	DIB@CNT/S	Freestanding	1.9–2.5	898	1.0 C/100		2.5	30	[170]
	MNWA/S	NF	4	854	3.2 mA cm ⁻² /400	0.07	10	6	[78]
	Co–N–CNTA/S	CFP	2	1045	1.0 C/1000	0.014	15		[65]
	NS–OCNA/S	Al foils	2.5	1175	1.0 C/600	0.1	6.7		[171]
	Co ₃ O ₄ /S	CC	4.1	621	2.0 C/500	0.047	4.1	5	[69]
	NCNT@Co–Co ₃ O ₄ @S	NF	4	737	2.0 C/500	0.023	10	15	[172]
	TiO ₂ /S	CC	1.7–2	699	1.0 C/300	0.072	2	>30	[173]
	Room-like TiO ₂ /S	Ti foils	2.8	~1000	0.5 mA cm ⁻² /400	0.05		20	[116]
	VO ₂ (P)–NCNT/S	Freestanding	4.8	~820	1.0 C/500	0.09	9.6	12	[114]
Transition metal oxide arrays	NiO/S	Stainless steel	2.5	1481	0.1 C/300		3.28	4.5	[174]
	NiCo ₂ O ₄ /S	CC	3.5	1280	0.2 C/200	0.24	8.9	6.7	[175]
	NiCo ₂ O ₄ /S	CC	1.1–1.3	1090	0.5 C/400	0.06	3.08		[176]
	ZnCo ₂ O ₄ /S	CC	2.2	1377	0.1 C/700	0.038	8.2		[177]
	NiCo ₂ S ₄ /S	NSCC	2	930	1.0 C/500	0.046	4.9	15	[121]
Transition metal sulfide arrays	FeCo ₂ S ₄ /S	CC	3.1–3.3	969	0.5 C/300	0.08	3.3	12	[60]
	Co ₉ S ₈ /S	Al foils		893.7	1.0 C/600	0.026			[61]
	Co ₉ S ₈ /S	CNF	1.2	908	1.0 C/1000	0.034	3.75	14	[178]
	CoS ₂ –CNA/S	CTNF	3.31	1013	1.0 C/100	0.13	7.19	30	[179]
	VS@NT/S	CP	1.2	818	2.0 C/1200	0.037	9.6	8	[67]
	ZnS _{1-x} /S	CC	2	659	1.0 C/500	0.04	5	5	[122]
	WS ₂ /S	Freestanding		1030	2.0 C/500	0.05			[180]
	CoZn/S	CC	1	1080	1.0 C/1800	0.04	9.2	3	[123]
	CoP/C/S	CC	1.81	923	2.0 C/600	0.016	4.17	30	[79]
	CoP@G/S	CC	2	1044.9	2.0 C/500	0.03	10.83	12	[181]
Transition metal phosphate arrays	CoP/NC/S	CC	1	867	1.0 C/560	0.033	1	>30	[127]
	FeP@C/S	CF	2.5	695	1.0 C/200	0.14	3.5	5	[128]
	VN/S	PCF	8.1	1310.8	0.1.0 C/250	0.07	8.1	20	[131]
	VN/Co/S	CC	1.7–2	750	1.0 C/500	0.063	7.8	12	[132]
	MOF–Co ₄ N/S	CC	1	~903	1.0 C/400	~0.044	1	>30	[133]
Transition metal nitride arrays	TiN/S	CC	1	1214	1.6 mA cm ⁻² /500	0.059	3	7	[130]

(Continued.)

Table 3. (Continued.)

Classification	Cathode	Substrate	Sulfur loading (mg cm^{-2})	Initial capacity (mA h g^{-1})	C rates /cycles	Capacity decay rate (%)	Sulfur loading (mg cm^{-2})	E/S ratio ($\mu\text{l mg}^{-1}$)	References
Heterostructure arrays	$\text{VO}_2(\text{p})\text{-V}_2\text{C/S}$	Al foils	1.8	1237	2.0 C/500	0.062	10.2	10	[141]
	$\text{V}_2\text{O}_5\text{-@V}_2\text{C/S}$	Freestanding	2	1138	0.5 C/1000	0.047	8.4	18	[182]
	$\text{Co}_9\text{S}_8\text{-Co}_4\text{N/S}$	CC	1.4–2	~620	5.0 C/1000	0.027	6.1	9.4	[143]
	$\text{MXene@TiO}_2\text{/S}$	Al foils	1.2	863	2.0 C/500	0.058	2.5	20	[183]
	$\text{MoS}_2\text{-MoN/S}$	Freestanding	1.2	~778	2.0 C/1000	0.041	12.2	4.2	[66]
	$\text{Co@CoO}_{1-x}\text{/S}$	CC	2	~600	2.0 C/400	0.023	5.1	14	[142]
	$\text{SnO}_2\text{-@MoS}_2\text{/S}$	CC	5	710	5.0 C/4000	0.009	5		[184]
	$\text{NiSe}_2\text{/S}$	CC	5	620	5.0 C/2000	0.019	12		[138]
Others	$\text{CoSe}_2\text{/S}$	CC	3	701	5.0 C/1000	0.026	5.1		[185]
	MoC@Ni/S	CFC	2	1238	0.5 C/300	0.062	6	7	[136]
	LaCO_3OH		1–1.2	900	1.0 C/1000	0.048			

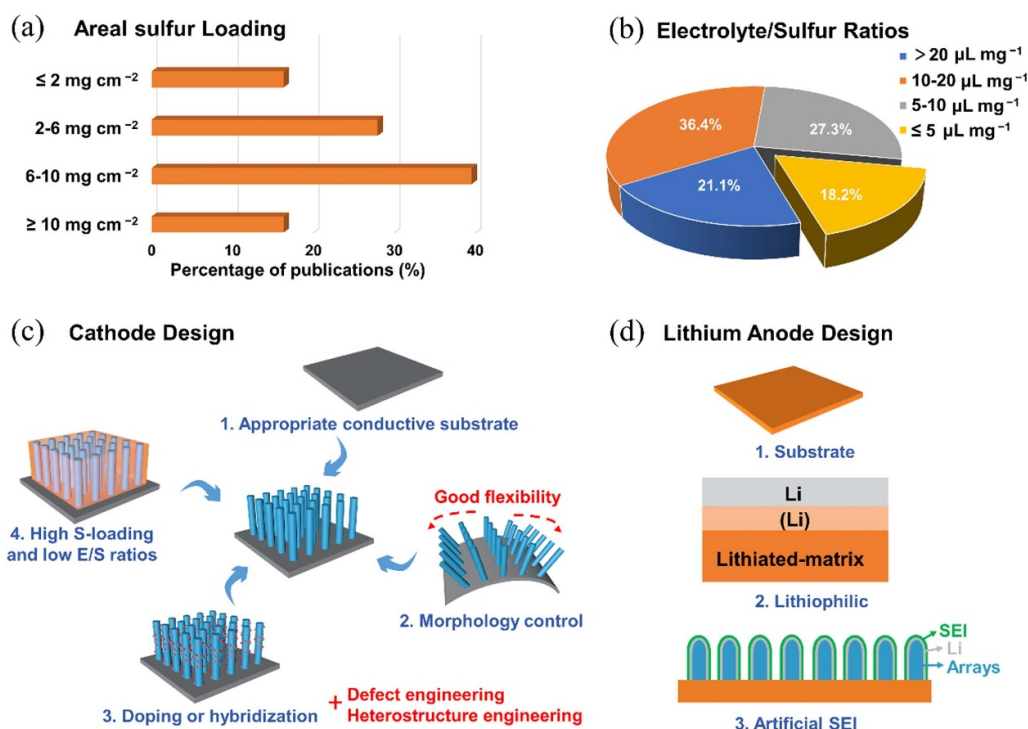


Figure 8. Challenges of designing NA electrodes. Statistical analysis of (a) areal sulfur loading, (b) electrolyte/sulfur ratio of the Li–S cells with NA structures. Rational design of NA electrodes for (c) sulfur cathode and (d) Li metal anode.

Table 4. Statistical analysis of areal sulfur loading of Li–S cells with nanoarray structures.

Areal sulfur loading	Amount	Percentage (%)
$\leq 2 \text{ mg cm}^{-2}$	7	16.3
2–6 mg cm^{-2}	17	39.5
6–10 mg cm^{-2}	12	27.9
$\geq 10 \text{ mg cm}^{-2}$	7	16.3

Table 5. Statistical analysis of electrolyte/sulfur ratio of Li–S cells with nanoarray structures.

Electrolyte/sulfur ratio	Amount	Percentage (%)
$> 20 \mu\text{L mg}^{-1}$	7	21.1
10–20 $\mu\text{L mg}^{-1}$	12	36.4
5–10 $\mu\text{L mg}^{-1}$	9	27.3
$\leq 5 \mu\text{L mg}^{-1}$	6	18.2

cell. In addition to reducing the E/S ratio to below $5 \mu\text{L mg}^{-1}$, cathode designs should also aim to lower the E/C ratio to below $5 \mu\text{L (mA h)}^{-1}$ in order to accurately evaluate and assess new advancements. The negative/positive (N/P) ratio defines the areal capacity of the Li anode in relation to the sulfur cathode. Conventional Li–S cells commonly use thick Li-foils ($> 500 \mu\text{m}$ or $\text{N/P} \geq 20$) as the anode, which reduces the specific energy of the cell. To address this limitation, employing thin Li-foils ($\text{N/P ratio} < 5$) can significantly improve both the gravimetric and volumetric energy density of the cell.

To further enhance the electrochemical performance of Li–S batteries using NAs in practical application, the following

research should attract much attention. For sulfur cathodes, several steps could be taken for the rational design of NA electrodes (figure 8(c)):

- (1) The selection of appropriate conductive substrate has a favorable synergistic effect with NAs, thus improving the electrochemical performance. The modification of the substrate is considered as an attractive approach, e.g., nitrogen–sulfur-doped carbon cloth [121], PCFs [131] and so on. It is very important for the substrates to have a rich porous structure that quickly transports electrons/ions, accommodates the maximum amount of sulfur, which ensures high sulfur loading and substrates containing cross-linked maze channels that physically immobilize the polysulfide species. The most commonly used substrates are expensive and provide high thickness, weight, and poor mechanical flexibility. Thus, it is important to develop advanced substrates that are inexpensive, highly compatible and with outstanding mechanical flexibility. Moreover, researchers should pay more attention to substrate-free electrodes which can reduce the whole mass/volume of electrodes, leading to a high energy density.
- (2) In the preparation of NAs materials, it is crucial to control their morphology accurately with effective and advanced synthetic approaches. Many 3D self-assembled nanostructures have been reported, but are difficult to apply in flexible energy storage devices due to random growth. Therefore, it remains a serious challenge to precisely control the morphology of NAs materials with suitable methods and templates. The architecture of the NA electrode

can be tailored to create a hierarchical or porous structure. This structure can provide a large surface area and interconnected pathways for the diffusion and immobilization of LiPSs, reducing their migration. It can also enhance the utilization of active materials and facilitate efficient electrochemical reactions.

- (3) Introducing specific materials within the NA structure that have high affinity for LiPSs can effectively trap and immobilize them. Various materials, such as doping or hybridization at atomic and molecular levels, the synergistic combination of structure strategy and defect engineering, and heterostructure engineering, have shown promising results in absorbing and trapping LiPSs. Incorporating these methods within the NA electrode can help mitigate the shuttle effect.
- (4) High sulfur loading and low E/S ratios are the key factors for realizing high-energy Li–S batteries. Designing 3D NA architectures with a large specific surface area and sufficient active sites is the most widely explored strategy to fabricate high-sulfur-loading cathodes. Actually, the electrode thickness should be thin enough to achieve superior rate performance, resulting in low sulfur loading. Therefore, it is still a key challenge to obtain a thicker layer in electrodes with good flexibility and high-rate capability. Moreover, it is necessary to achieve low E/S ratios by adjusting the inner porosity and wetting properties.

For Li metal anodes, the following steps could be followed towards the rational design of NA electrodes (figure 8(d)):

- (1) Most substrates such as metal foil and metal foam that mostly support NAs are too expensive and add too much volume and weight. Therefore, it is necessary to develop advanced substrates with low price, strong environmental flexibility and good mechanical stability for improving the performance of batteries.
- (2) Electrodes with excellent lithiophilicity can direct uniform Li nucleation, suppress dendritic Li growth, and improve cycling along with coulombic efficiency. Thus, it is essential to design lithiophilic NA structures for Li metal anodes with a low Li nucleation barrier, dendrite-free morphology, and safe batteries with Li metal anodes.
- (3) Research into artificial SEI is extremely important and should be highly valued. In addition to the common requirements of SEI, such as uniformity, fast ion transport, mechanical strength, the effect of polysulfides on the SEI needs further consideration and rational design. The shuttling effect of polysulfides is the most serious obstacle hindering practical applications of Li–S batteries. Therefore, researchers should pay more attention to determining anode protective structures that can protect lithium metal against dissolved polysulfides. Additionally, constructing SEI that can reject polysulfides may be a promising strategy.

Stability plays a significant role in determining the long-term performance and cycle life of the battery system.

The following guidelines should be followed to ensure stability in the design of both the sulfur cathode and lithium anode:

- (1) Substrate design - select a substrate that offers mechanical support and stability to the array electrodes. Consider using flexible or rigid substrates that can withstand the expansion and contraction of the electrode materials during cycling.
- (2) Material selection - choose materials with excellent mechanical properties and chemical stability. Consider materials that can withstand the stress and strain experienced during cycling and that exhibit high chemical resistance to the electrolyte.
- (3) Electrode architecture - design hierarchical or interconnected structures to provide mechanical support and minimize electrode deformation.
- (4) Electrode thickness - control the thickness of the array electrodes to strike a balance between maximizing active material loading and maintaining structural stability. Thick electrodes may enhance capacity, but they can also increase mechanical stress and strain, leading to degradation.

There has been significant progress in the development of NA electrodes for Li–S pouch cells. NA electrodes have emerged as a promising approach to enhance the performance of Li–S batteries by addressing some of the key challenges associated with this technology, such as low cycling stability and poor sulfur utilization. Despite the progress, there are still some challenges that need to be addressed before NA electrodes can be effectively implemented in commercial Li–S pouch cells. One of the major challenges is the stability of the NA structure over long cycling periods. Maintaining the structural integrity of the NA electrodes and preventing their degradation is crucial for the long-term performance and durability of Li–S batteries.

6. Future perspectives

Li–S batteries are regarded as the most promising candidates for energy storage devices due to their high theoretical energy density. The fabrication of effective and stable catalysts is crucial for the realization of high-performance Li–S batteries. NA electrodes have exhibited marvelous electrochemical performance and durability due to their features of having no binders/additives, a large number of active sites, high sulfur loading, facile electron/ion transport, and a stable structure for buffering volume changes. In this review, we comprehensively elaborate the progress and development of NA structures starting with the advantages of NAs materials, principles of fabrication and synthetic methods, along with applications for the sulfur cathode, separator and lithium metal anode of Li–S batteries. In short, this review provides an in-depth analysis of the challenges and rational design of NA structures for Li–S batteries.

Despite the fact that great progress has been made in the fabrication of NA structures for sulfur cathodes, lithium anodes, and functional separators, enormous challenges and

opportunities remain in advancing practical Li–S batteries. We should always adhere to the ‘five 5 s’ design guidelines: sulfur loading $>5 \text{ mg cm}^{-2}$, carbon content $<5\%$, E/S ratio $<5 \text{ ml mg}^{-1}$ and E/C ratio $<5 \text{ ml (mA h)}^{-1}$, as they serve as the minimum standard for achieving a lightweight and compact high-energy system. While most NA electrodes can achieve a high sulfur loading, they need to be wetted with a large amount of electrolyte in order to form ion channels within the electrode. Thus, the E/S ratio and E/C ratio must be taken seriously to simultaneously achieve outstanding electrochemical performance and energy density. The development of NA electrodes holds promise for high-energy Li–S pouch cells. By improving sulfur utilization and cycling stability, NA electrodes have the potential to significantly increase the energy density and lifespan of Li–S batteries. However, further research is needed to optimize the design, materials, and manufacturing processes of NA electrodes to ensure their practical viability and scalability.

Furthermore, it is of critical importance to understand the scientific mechanism such as electrochemical process, electrode degradation, etc in Li–S systems which be helpful in further improvement of overall battery performance. The phase transitions, volume changes, and side reactions that take place during the charge/discharge process may all be precisely monitored using the NA structures, which can assist to remove the interference of binders and additives in conventional electrodes. Therefore, based on the NA structure electrodes, it is effective to explore the energy storage processes and mechanisms using advanced characterization techniques and computational simulations.

In addition, (quasi) solid state electrolytes energy storage devices based on NA structures are also very promising. With suitable interspacing between orderly formed nanostructures, NA structures electrodes can achieve more adequate electrolyte penetration, resulting in tight interfacial contact with solid-state electrolytes, as opposed to the limited contact in conventional powder electrodes. Therefore, (quasi) solid state Li–S batteries based on NA structures need to be further studied.

Acknowledgments

This study was financially supported by Beijing Municipal Natural Science Foundation-Xiaomi Innovation Joint Fund (L223011), the National Natural Science Foundation of China (Nos. 21771018, 21875004, 22108149), China Postdoctoral Science Foundation (No. 2021M691755), Beijing University of Chemical Technology (buctrc201901).

ORCID iD

Wen Liu  <https://orcid.org/0000-0001-8884-7799>

References

- [1] Wu F, Maier J and Yu Y 2020 Guidelines and trends for next-generation rechargeable lithium and lithium-ion batteries *Chem. Soc. Rev.* **49** 1569–614
- [2] Liu J *et al* 2019 Pathways for practical high-energy long-cycling lithium metal batteries *Nat. Energy* **4** 180–6
- [3] Huang Z, Zhang R, Zhang S, Li P, Li C and Zhi C 2022 Recent advances and future perspectives for aqueous zinc-ion capacitors *Mater. Futures* **1** 022101
- [4] Zhao Y, Zhang P, Liang J, Xia X, Ren L, Song L, Liu W and Sun X 2022 Unlocking layered double hydroxide as a high-performance cathode material for aqueous zinc-ion batteries *Adv. Mater.* **34** 2204320
- [5] Liu J, Ren L, Wang Y, Lu X, Zhou M and Liu W 2023 A highly-stable bifunctional NiCo_2S_4 nanoarray@carbon paper electrode for aqueous polysulfide/iodide redox flow battery *J. Power Sources* **561** 232607
- [6] Tong B, Song Z, Wu H, Wang X, Feng W, Zhou Z and Zhang H 2022 Ion transport and structural design of lithium-ion conductive solid polymer electrolytes: a perspective *Mater. Futures* **1** 042103
- [7] Fu S *et al* 2021 Ultrathin [110]-confined $\text{Li}_4\text{Ti}_5\text{O}_{12}$ nanoflakes for high rate lithium storage *Adv. Energy Mater.* **11** 2003270
- [8] Wu Y *et al* 2021 In-built ultraconformal interphases enable high-safety practical lithium batteries *Energy Storage Mater.* **43** 248–57
- [9] Goodenough J B and Park K-S 2013 The Li-ion rechargeable battery: a perspective *J. Am. Chem. Soc.* **135** 1167–76
- [10] Pang Q, Liang X, Kwok C Y and Nazar L F 2016 Advances in lithium–sulfur batteries based on multifunctional cathodes and electrolytes *Nat. Energy* **1** 16132
- [11] Manthiram A, Fu Y, Chung S, Zu C and Su Y 2014 Rechargeable lithium–sulfur batteries *Chem. Rev.* **114** 11751–87
- [12] Ren L, Liu J, Zhao Y, Wang Y, Lu X, Zhou M, Zhang G, Liu W, Xu H and Sun X 2023 Regulating electronic structure of Fe-N_4 single atomic catalyst via neighboring sulfur doping for high performance lithium–sulfur batteries *Adv. Funct. Mater.* **33** 2210509
- [13] Seh Z W, Sun Y, Zhang Q and Cui Y 2016 Designing high-energy lithium–sulfur batteries *Chem. Soc. Rev.* **45** 5605–34
- [14] Qiao L, Ren L, Zhang R, Chen J, Xu M, Liu J, Xu H, Liu W, Chang Z and Sun X 2021 Hollow carbon spheres embedded with VN quantum dots as an efficient cathode host for lithium–sulfur batteries *Energy Fuels* **35** 10219–26
- [15] Zhang L, Qin X, Zhao S, Wang A, Luo J, Wang Z L, Kang F, Lin Z and Li B 2020 Advanced matrixes for binder-free nanostructured electrodes in lithium-ion batteries *Adv. Mater.* **32** 1908445
- [16] Zhang H, Ono L K, Tong G, Liu Y and Qi Y 2021 Long-life lithium-sulfur batteries with high areal capacity based on coaxial CNTs@ TiN-TiO_2 sponge *Nat. Commun.* **12** 4738
- [17] Li J, Cai Y, Wu H, Yu Z, Yan X, Zhang Q, Gao T Z, Liu K, Jia X and Bao Z 2021 Polymers in lithium-ion and lithium metal batteries *Adv. Energy Mater.* **11** 2003239
- [18] Ji X, Lee K T and Nazar L F 2009 A highly ordered nanostructured carbon–sulphur cathode for lithium–sulphur batteries *Nat. Mater.* **8** 500–6
- [19] Zheng M, Chi Y, Hu Q, Tang H, Jiang X, Zhang L, Zhang S, Pang H and Xu Q 2019 Carbon nanotube-based materials for lithium–sulfur batteries *J. Mater. Chem. A* **7** 17204–41

- [20] Fang R, Chen K, Yin L, Sun Z, Li F and Cheng H M 2019 The regulating role of carbon nanotubes and graphene in lithium-ion and lithium-sulfur batteries *Adv. Mater.* **31** 1800863
- [21] Duan H, Li K, Xie M, Chen J, Zhou H, Wu X, Ning G, Cooper A I and Li D 2021 Scalable synthesis of ultrathin polyimide covalent organic framework nanosheets for high-performance lithium-sulfur batteries *J. Am. Chem. Soc.* **143** 19446–53
- [22] Chen C, Liang Q, Wang G, Liu D and Xiong X 2022 Grain-boundary-rich artificial SEI layer for high-rate lithium metal anodes *Adv. Funct. Mater.* **32** 2107249
- [23] Huang J, Liu J, He J, Wu M, Qi S, Wang H, Li F and Ma J 2021 Optimizing electrode/electrolyte interphases and Li-ion flux/solvation for lithium-metal batteries with qua-functional heptafluorobutyric anhydride *Angew. Chem.* **133** 20885–90
- [24] Li F, He J, Liu J, Wu M, Hou Y, Wang H, Qi S, Liu Q, Hu J and Ma J 2021 Gradient solid electrolyte interphase and lithium-ion solvation regulated by bisfluoroacetamide for stable lithium metal batteries *Angew. Chem., Int. Ed.* **60** 6600–8
- [25] Ren L, Wang Q, Li Y, Hu C, Zhao Y, Qiao L, Zhou H, Liu W, Xu H and Sun X 2021 Catalytic separators with Co–N–C nanoreactors for high-performance lithium-sulfur batteries *Inorg. Chem. Front.* **8** 3066–76
- [26] Hu Y, Chen W, Lei T, Jiao Y, Wang H, Wang X, Rao G, Wang X, Chen B and Xiong J 2020 Graphene quantum dots as the nucleation sites and interfacial regulator to suppress lithium dendrites for high-loading lithium-sulfur battery *Nano Energy* **68** 104373
- [27] Fu S, Chen J, Wang X, He Q, Tong S and Wu M 2020 Free-standing crystalline@ amorphous core-shell nanoarrays for efficient energy storage *Small* **16** 2000040
- [28] Chao D *et al* 2016 Array of nanosheets render ultrafast and high-capacity Na-ion storage by tunable pseudocapacitance *Nat. Commun.* **7** 12122
- [29] Jiang J, Li Y, Liu J, Huang X, Yuan C and Lou X W 2012 Recent advances in metal oxide-based electrode architecture design for electrochemical energy storage *Adv. Mater.* **24** 5166–80
- [30] Jiang J, Li Y, Liu J and Huang X 2011 Building one-dimensional oxide nanostructure arrays on conductive metal substrates for lithium-ion battery anodes *Nanoscale* **3** 45–58
- [31] Chan C K, Zhang X F and Cui Y 2008 High capacity Li ion battery anodes using Ge nanowires *Nano Lett.* **8** 307–9
- [32] Black R, Oh S H, Lee J-H, Yim T, Adams B and Nazar L F 2012 Screening for superoxide reactivity in Li-O₂ batteries: effect on Li₂O₂/LiOH crystallization *J. Am. Chem. Soc.* **134** 2902–5
- [33] Singh S K, Takeyasu K and Nakamura J 2019 Active sites and mechanism of oxygen reduction reaction electrocatalysis on nitrogen-doped carbon materials *Adv. Mater.* **31** 1804297
- [34] Zhang J, Li P, Wang Z, Qiao J, Rooney D, Sun W and Sun K 2015 Three-dimensional graphene-Co₃O₄ cathodes for rechargeable Li-O₂ batteries *J. Mater. Chem. A* **3** 1504–10
- [35] Urbonaite S, Poux T and Novák P 2015 Progress towards commercially viable Li-S battery cells *Adv. Energy Mater.* **5** 1500118
- [36] Fang R, Zhao S, Sun Z, Wang D, Cheng H and Li F 2017 More reliable lithium-sulfur batteries: status, solutions and prospects *Adv. Mater.* **29** 1606823
- [37] Chen Y, Wang T, Tian H, Su D, Zhang Q and Wang G 2021 Advances in lithium-sulfur batteries: from academic research to commercial viability *Adv. Mater.* **33** 2003666
- [38] Ni J and Li L 2020 Cathode architectures for rechargeable ion batteries: progress and perspectives *Adv. Mater.* **32** 2000288
- [39] Liu F *et al* 2018 Upgrading traditional liquid electrolyte via *in situ* gelation for future lithium metal batteries *Sci. Adv.* **4** eaat5383
- [40] Chen X, He W, Ding L, Wang S and Wang H 2019 Enhancing interfacial contact in all solid state batteries with a cathode-supported solid electrolyte membrane framework *Energy Environ. Sci.* **12** 938–44
- [41] Liu Z, Mo F, Li H, Zhu M, Wang Z, Liang G and Zhi C 2018 Advances in flexible and wearable energy-storage textiles *Small Methods* **2** 1800124
- [42] Lin D, Liu Y and Cui Y 2017 Reviving the lithium metal anode for high-energy batteries *Nat. Nanotechnol.* **12** 194–206
- [43] Zhong Y, Chen Y, Cheng Y, Fan Q, Zhao H, Shao H, Lai Y, Shi Z, Ke X and Guo Z 2019 Li alginate-based artificial SEI layer for stable lithium metal anodes *ACS Appl. Mater. Interfaces* **11** 37726–31
- [44] Li N W, Shi Y, Yin Y X, Zeng X X, Li J Y, Li C J, Wan L J, Wen R and Guo Y G 2018 A flexible solid electrolyte interphase layer for long-life lithium metal anodes *Angew. Chem.* **130** 1521–5
- [45] Zhang Y *et al* 2017 High-capacity, low-tortuosity, and channel-guided lithium metal anode *Proc. Natl Acad. Sci.* **114** 3584–9
- [46] Zheng Z, Su Q, Zhang Q, Hu X, Yin Y, Wen R, Ye H, Wang Z and Guo Y 2019 Low volume change composite lithium metal anodes *Nano Energy* **64** 103910
- [47] Duan H, Yin Y, Shi Y, Wang P, Zhang X, Yang C, Shi J, Wen R, Guo Y and Wan L 2018 Dendrite-free Li-metal battery enabled by a thin asymmetric solid electrolyte with engineered layers *J. Am. Chem. Soc.* **140** 82–85
- [48] Liu S, Xia X, Zhong Y, Deng S, Yao Z, Zhang L, Cheng X B, Wang X, Zhang Q and Tu J 2018 3D TiC/C core/shell nanowire skeleton for dendrite-free and long-life lithium metal anode *Adv. Energy Mater.* **8** 1702322
- [49] Zheng Z, Ye H and Guo Z 2020 Recent progress in designing stable composite lithium anodes with improved wettability *Adv. Sci.* **7** 2002212
- [50] Li Y-N, Wang C-Y, Gao R-M, Cao F-F and Ye H 2021 Recent smart lithium anode configurations for high-energy lithium metal batteries *Energy Storage Mater.* **38** 262–75
- [51] Lin D, Liu Y, Pei A and Cui C 2017 Nanoscale perspective: materials designs and understandings in lithium metal anodes *Nano Res.* **10** 4003–26
- [52] Gu J, Chen H, Shi Y, Cao Z, Du Z, Li B and Yang S 2022 Eliminating lightning-rod effect of lithium anodes via sine-wave analogous MXene layers *Adv. Energy Mater.* **12** 2201181
- [53] Gao X, Zhang H, Li Q, Yu X, Hong Z, Zhang X, Liang C and Lin Z 2016 Hierarchical NiCo₂O₄ hollow microcuboids as bifunctional electrocatalysts for overall water-splitting *Angew. Chem., Int. Ed.* **55** 6290–4
- [54] Hou J, Wu Y, Zhang B, Cao S, Li Z and Sun L 2019 Rational design of nanoarray architectures for electrocatalytic water splitting *Adv. Funct. Mater.* **29** 1808367
- [55] Huang Y, Quan L, Liu T, Chen Q, Cai D and Zhan H 2018 Construction of MOF-derived hollow Ni–Zn–Co–S nanosword arrays as binder-free electrodes for asymmetric supercapacitors with high energy density *Nanoscale* **10** 14171–81
- [56] Deng S, Zhong Y, Zeng Y, Wang Y, Wang X, Lu X, Xia X and Tu J 2018 Hollow TiO₂@Co₉S₈ core-branch arrays as bifunctional electrocatalysts for efficient oxygen/hydrogen production *Adv. Sci.* **5** 1700772

- [57] Zhu C, Wang H and Guan C 2020 Recent progress on hollow array architectures and their applications in electrochemical energy storage *Nanoscale Horiz.* **5** 1188–99
- [58] Lee J, Llerena Zambrano B, Woo J, Yoon K and Lee T 2020 Recent advances in 1D stretchable electrodes and devices for textile and wearable electronics: materials, fabrications, and applications *Adv. Mater.* **32** 1902532
- [59] Lu X, Wang H, Liu X, Song Z, Jiang N, Xie F, Zheng Q and Lin D 2020 Functional separators prepared via *in-situ* growth of hollow CoSO_4 hydrate arrays on pristine polypropylene membrane for high performance lithium–sulfur batteries *J. Alloys Compd.* **838** 155618
- [60] Guo B, Bandaru S, Dai C, Chen H, Zhang Y, Xu Q, Bao S, Chen M and Xu M 2018 Self-supported FeCo_2S_4 nanotube arrays as binder-free cathodes for lithium–sulfur batteries *ACS Appl. Mater. Interfaces* **10** 43707–15
- [61] Dai C, Lim J M, Wang M, Hu L, Chen Y, Chen Z, Chen H, Bao S J, Shen B and Li Y 2018 Honeycomb-like spherical cathode host constructed from hollow metallic and polar Co_9S_8 tubules for advanced lithium–sulfur batteries *Adv. Funct. Mater.* **28** 1704443
- [62] Tang W, Wang X, Xie D, Xia X, Gu C and Tu J 2018 Hollow metallic 1T MoS_2 arrays grown on carbon cloth: a freestanding electrode for sodium ion batteries *J. Mater. Chem. A* **6** 18318–24
- [63] Shao Y, El-Kady M F, Sun J, Li Y, Zhang Q, Zhu M, Wang H, Dunn B and Kaner R B 2018 Design and mechanisms of asymmetric supercapacitors *Chem. Rev.* **118** 9233–80
- [64] Chen X, Yang H, Liu G, Gao F, Dai M, Hu Y, Chen H, Cao W, Hu P and Hu W 2018 Hollow spherical nanoshell arrays of 2D layered semiconductor for high-performance photodetector device *Adv. Funct. Mater.* **28** 1705153
- [65] Hu C *et al* 2019 An entangled cobalt–nitrogen–carbon nanotube array electrode with synergetic confinement and electrocatalysis of polysulfides for stable Li–S batteries *ACS Appl. Energy Mater.* **2** 2904–12
- [66] Wang S *et al* 2021 Insight into MoS_2 – MoN heterostructure to accelerate polysulfide conversion toward high-energy-density lithium–sulfur batteries *Adv. Energy Mater.* **11** 2003314
- [67] Wang S *et al* 2019 Efficient trapping and catalytic conversion of polysulfides by VS_4 nanosites for Li–S batteries *ACS Energy Lett.* **4** 755–62
- [68] Xu X, Yang Q, Wattanatorn N, Zhao C, Chiang N, Jonas S J and Weiss P S 2017 Multiple-patterning nanosphere lithography for fabricating periodic three-dimensional hierarchical nanostructures *ACS Nano* **11** 10384–91
- [69] Xia X, Tu J, Mai Y, Wang X, Gu C and Zhao X 2011 Self-supported hydrothermal synthesized hollow Co_3O_4 nanowire arrays with high supercapacitor capacitance *J. Mater. Chem.* **21** 9319–25
- [70] Tang Z, Zhang G, Zhang H, Wang L, Shi H, Wei D and Duan H 2018 MOF-derived N-doped carbon bubbles on carbon tube arrays for flexible high-rate supercapacitors *Energy Storage Mater.* **10** 75–84
- [71] Li F, Xu R, Li Y, Liang F, Zhang D, Fu W and Lv X 2019 N-doped carbon coated NiCo_2S_4 hollow nanotube as bifunctional electrocatalyst for overall water splitting *Carbon* **145** 521–8
- [72] Liu Z, Zhao W, Kumar P, Li X, Al Wahedi Y, Mkhoyan K A, Tsapatsis M and Stein A 2018 Direct synthesis and pseudomorphic transformation of mixed metal oxide nanostructures with non-close-packed hollow sphere arrays *Angew. Chem.* **130** 15933–7
- [73] Zhou G, Wang D, Li F, Hou P, Yin L, Liu C, Lu G Q M, Gentle I R and Cheng H 2012 A flexible nanostructured sulphur–carbon nanotube cathode with high rate performance for Li–S batteries *Energy Environ. Sci.* **5** 8901–6
- [74] Li S, Xia X, Wang X and Tu J 2016 Free-standing sulfur cathodes composited with carbon nanorods arrays for Li–S batteries application *Mater. Res. Bull.* **83** 474–80
- [75] Yin P *et al* 2016 Single cobalt atoms with precise N-coordination as superior oxygen reduction reaction catalysts *Angew. Chem.* **128** 10958–63
- [76] Wang X *et al* 2016 Directly converting Fe-doped metal–organic frameworks into highly active and stable Fe-NC catalysts for oxygen reduction in acid *Nano Energy* **25** 110–9
- [77] Yi F Y, Zhang R, Wang H, Chen L F, Han L, Jiang H L and Xu Q 2017 Metal–organic frameworks and their composites: synthesis and electrochemical applications *Small Methods* **1** 1700187
- [78] Yang X *et al* 2018 Multi-functional nanowall arrays with unrestricted Li^+ transport channels and an integrated conductive network for high-areal-capacity Li–S batteries *J. Mater. Chem. A* **6** 22958–65
- [79] Wang Z *et al* 2019 Self-supported and flexible sulfur cathode enabled via synergistic confinement for high-energy-density lithium–sulfur batteries *Adv. Mater.* **31** 1902228
- [80] He J, Chen Y and Manthiram A 2018 Vertical Co_9S_8 hollow nanowall arrays grown on a Celgard separator as a multifunctional polysulfide barrier for high-performance Li–S batteries *Energy Environ. Sci.* **11** 2560–8
- [81] Zhang W, Yan X, Tong X, Yang J, Miao L, Sun Y and Peng L 2016 Synthesis of nickel sulfide monolayer hollow spheres arrays as cathode materials for alkaline batteries *Mater. Lett.* **178** 120–3
- [82] Poongodi S, Kumar P S, Mangalaraj D, Ponpandian N, Meena P, Masuda Y and Lee C 2017 Electrodeposition of WO_3 nanostructured thin films for electrochromic and H_2S gas sensor applications *J. Alloys Compd.* **719** 71–81
- [83] Zhuo S, Shi Y, Liu L, Li R, Shi L, Anjum D H, Han Y and Wang P 2018 Dual-template engineering of triple-layered nanowall electrode of metal chalcogenides sandwiched with hydrogen-substituted graphdiyne *Nat. Commun.* **9** 3132
- [84] Zhao Y, Mu S, Sun W, Liu Q, Li Y, Yan Z, Huo Z and Liang W 2016 Growth of copper oxide nanocrystals in metallic nanotubes for high performance battery anodes *Nanoscale* **8** 19994–20000
- [85] Niu C *et al* 2015 General synthesis of complex nanotubes by gradient electrospinning and controlled pyrolysis *Nat. Commun.* **6** 7402
- [86] Elias J, Lévy-Clément C, Bechelany M, Michler J, Wang G-Y, Wang Z and Philippe L 2010 Hollow urchin-like ZnO thin films by electrochemical deposition *Adv. Mater.* **22** 1607–12
- [87] Xia X, Chao D, Qi X, Xiong Q, Zhang Y, Tu J, Zhang H and Fan H J 2013 Controllable growth of conducting polymers shell for constructing high-quality organic/inorganic core/shell nanostructures and their optical-electrochemical properties *Nano Lett.* **13** 4562–8
- [88] Li B, Li S, Liu J, Wang B and Yang S 2015 Vertically aligned sulfur–graphene nanowalls on substrates for ultrafast lithium–sulfur batteries *Nano Lett.* **15** 3073–9
- [89] Yuan S, Huang X L, Ma D L, Wang H G, Meng F Z and Zhang X B 2014 Engraving copper foil to give large-scale binder-free porous CuO arrays for a high-performance sodium-ion battery anode *Adv. Mater.* **26** 2273–9
- [90] Zuo W, Zhu W, Zhao D, Sun Y, Li Y, Liu J and Lou X W D 2016 Bismuth oxide: a versatile high-capacity electrode material for rechargeable aqueous metal-ion batteries *Energy Environ. Sci.* **9** 2881–91

- [91] Liu J, Song K, van Aken P A, Maier J and Yu Y 2014 Self-supported $\text{Li}_4\text{Ti}_5\text{O}_{12}$ -C nanotube arrays as high-rate and long-life anode materials for flexible Li-ion batteries *Nano Lett.* **14** 2597–603
- [92] Liu S, Hong X, Wang D, Li Y, Xu J, Zheng C and Xie K 2018 Hollow carbon spheres with nanoporous shells and tailored chemical interfaces as sulfur host for long cycle life of lithium sulfur batteries *Electrochim. Acta* **279** 10–18
- [93] Hernández-Rentero C, Córdoba R, Moreno N, Caballero A, Morales J, Olivares-Marín M and Gómez-Serrano V 2018 Low-cost disordered carbons for Li/S batteries: a high-performance carbon with dual porosity derived from cherry pits *Nano Res.* **11** 89–100
- [94] Liang J, Sun Z, Li F and Cheng H 2016 Carbon materials for Li-S batteries: functional evolution and performance improvement *Energy Storage Mater.* **2** 76–106
- [95] Zheng G, Yang Y, Cha J J, Hong S S and Cui Y 2011 Hollow carbon nanofiber-encapsulated sulfur cathodes for high specific capacity rechargeable lithium batteries *Nano Lett.* **11** 4462–7
- [96] Reddy A L M, Shaijumon M M, Gowda S R and Ajayan P M 2009 Coaxial MnO_2 /carbon nanotube array electrodes for high-performance lithium batteries *Nano Lett.* **9** 1002–6
- [97] Park S-K, Lee J, Hwang T, Jang B and Piao Y 2017 Scalable synthesis of honeycomb-like ordered mesoporous carbon nanosheets and their application in lithium–sulfur batteries *ACS Appl. Mater. Interfaces* **9** 2430–8
- [98] Ni J and Li L 2018 Self-supported 3D array electrodes for sodium microbatteries *Adv. Funct. Mater.* **28** 1704880
- [99] Zhou G, Paek E, Hwang G S and Manthiram A 2015 Long-life Li/polysulphide batteries with high sulphur loading enabled by lightweight three-dimensional nitrogen/sulphur-codoped graphene sponge *Nat. Commun.* **6** 7760
- [100] Jin C, Zhang W, Zhuang Z, Wang J, Huang H, Gan Y, Xia Y, Liang C, Zhang J and Tao X 2017 Enhanced sulfide chemisorption using boron and oxygen dually doped multi-walled carbon nanotubes for advanced lithium–sulfur batteries *J. Mater. Chem. A* **5** 632–40
- [101] Song J, Yu Z, Gordin M L and Wang D 2016 Advanced sulfur cathode enabled by highly crumpled nitrogen-doped graphene sheets for high-energy-density lithium–sulfur batteries *Nano Lett.* **16** 864–70
- [102] Liang C, Dudney N J and Howe J Y 2009 Hierarchically structured sulfur/carbon nanocomposite material for high-energy lithium battery *Chem. Mater.* **21** 4724–30
- [103] Wei Seh Z, Li W, Cha J J, Zheng G, Yang Y, McDowell M T, Hsu P-C and Cui Y 2013 Sulphur– TiO_2 yolk–shell nanoarchitecture with internal void space for long-cycle lithium–sulphur batteries *Nat. Commun.* **4** 1331
- [104] Mei S, Jafta C J, Lauermaun I, Ran Q, Kärger M, Ballauff M and Lu Y 2017 Porous Ti_4O_7 particles with interconnected-pore structure as a high-efficiency polysulfide mediator for lithium–sulfur batteries *Adv. Funct. Mater.* **27** 1701176
- [105] Li Z, Guan B Y, Zhang J and Lou X W D 2017 A compact nanoconfined sulfur cathode for high-performance lithium-sulfur batteries *Joule* **1** 576–87
- [106] Rehman S, Tang T, Ali Z, Huang X and Hou Y 2017 Integrated design of MnO_2 @carbon hollow nanoboxes to synergistically encapsulate polysulfides for empowering lithium sulfur batteries *Small* **13** 1700087
- [107] Luo D *et al* 2019 Synergistic engineering of defects and architecture in binary metal chalcogenide toward fast and reliable lithium–sulfur batteries *Adv. Energy Mater.* **9** 1900228
- [108] Ji X, Evers S, Black R and Nazar L F 2011 Stabilizing lithium–sulphur cathodes using polysulphide reservoirs *Nat. Commun.* **2** 325
- [109] Liang X, Kwok C Y, Lodi-Marzano F, Pang Q, Cuisinier M, Huang H, Hart C J, Houtarde D, Kaup K and Sommer H 2016 Tuning transition metal oxide–sulfur interactions for long life lithium sulfur batteries: the “Goldilocks” principle *Adv. Energy Mater.* **6** 1501636
- [110] Fan Q, Liu W, Weng Z, Sun Y and Wang H 2015 Ternary hybrid material for high-performance lithium–sulfur battery *J. Am. Chem. Soc.* **137** 12946–53
- [111] Zhao C, Shen C, Xin F, Sun Z and Han W 2014 Prussian blue-derived Fe_2O_3 /sulfur composite cathode for lithium–sulfur batteries *Mater. Lett.* **137** 52–55
- [112] Cheng H, Wang S, Tao D and Wang M 2014 Sulfur/ Co_3O_4 nanotube composite with high performances as cathode materials for lithium sulfur batteries *Funct. Mater. Lett.* **7** 1450020
- [113] Liang X, Hart C, Pang Q, Garsuch A, Weiss T and Nazar L F 2015 A highly efficient polysulfide mediator for lithium–sulfur batteries *Nat. Commun.* **6** 5682
- [114] Wang S *et al* 2019 Designing a highly efficient polysulfide conversion catalyst with paramontroseite for high-performance and long-life lithium–sulfur batteries *Nano Energy* **57** 230–40
- [115] Chang Z, Dou H, Ding B, Wang J, Wang Y, Hao X and MacFarlane D R 2017 Co_3O_4 nanoneedle arrays as a multifunctional “super-reservoir” electrode for long cycle life Li–S batteries *J. Mater. Chem. A* **5** 250–7
- [116] Guo J, Zhao S, Shen Y, Shao G and Zhang F 2020 “Room-like” TiO_2 array as a sulfur host for lithium–sulfur batteries: combining advantages of array and closed structures *ACS Sustain. Chem. Eng.* **8** 7609–16
- [117] Yuan Z, Peng H, Hou T, Huang J, Chen C, Wang D, Cheng X, Wei F and Zhang Q 2016 Powering lithium–sulfur battery performance by propelling polysulfide redox at sulfiphilic hosts *Nano Lett.* **16** 519–27
- [118] Chen T *et al* 2017 Metallic and polar Co_9S_8 inlaid carbon hollow nanopolyhedra as efficient polysulfide mediator for lithium–sulfur batteries *Nano Energy* **38** 239–48
- [119] Wang H, Zhang Q, Yao H, Liang Z, Lee H-W, Hsu P-C, Zheng G and Cui Y 2014 High electrochemical selectivity of edge versus terrace sites in two-dimensional layered MoS_2 materials *Nano Lett.* **14** 7138–44
- [120] Lei T, Chen W, Huang J, Yan C, Sun H, Wang C, Zhang W, Li Y and Xiong J 2017 Multi-functional layered WS_2 nanosheets for enhancing the performance of lithium–sulfur batteries *Adv. Energy Mater.* **7** 1601843
- [121] Sun T, Huang C, Shu H, Luo L, Liang Q, Chen M, Su J and Wang X 2020 Porous NiCo_2S_4 nanoneedle arrays with highly efficient electrocatalysis anchored on carbon cloths as self-supported hosts for high-loading Li–S batteries *ACS Appl. Mater. Interfaces* **12** 57975–86
- [122] Wang J, Zhao Y, Li G, Luo D, Liu J, Zhang Y, Wang X, Shui L and Chen Z 2021 Aligned sulfur-deficient ZnS_{1-x} nanotube arrays as efficient catalyzer for high-performance lithium/sulfur batteries *Nano Energy* **84** 105891
- [123] Ye Z, Jiang Y, Li L, Wu F and Chen R 2022 Synergetic anion vacancies and dense heterointerfaces into bimetal chalcogenide nanosheet arrays for boosting electrocatalysis sulfur conversion *Adv. Mater.* **34** 2109552
- [124] Abdelkader A A, Rodene D D, Norouzi N, Alzharani A, Weeraratne K S, Gupta R B and El-Kaderi H M 2020 Multifunctional electrocatalytic cathodes derived from metal–organic frameworks for advanced lithium-sulfur batteries *Chem. Eur. J.* **26** 13896–903
- [125] Huang S, von Lim Y, Zhang X, Wang Y, Zheng Y, Kong D, Ding M, Yang S A and Yang H Y 2018 Regulating the polysulfide redox conversion by iron phosphide nanocrystals for high-rate and ultrastable lithium–sulfur battery *Nano Energy* **51** 340–8

- [126] Luo Y, Luo N, Kong W, Wu H, Wang K, Fan S, Duan W and Wang J 2018 Multifunctional interlayer based on molybdenum diphosphide catalyst and carbon nanotube film for lithium–sulfur batteries *Small* **14** 1702853
- [127] Xiao K, Chen Z, Liu Z, Zhang L, Cai X, Song C, Fan Z, Chen X, Liu J and Shen Z X 2020 N-doped carbon sheets arrays embedded with CoP nanoparticles as high-performance cathode for Li–S batteries via triple synergistic effects *J. Power Sources* **455** 227959
- [128] Shen J *et al* 2019 Mechanistic understanding of metal phosphide host for sulfur cathode in high-energy-density lithium–sulfur batteries *ACS Nano* **13** 8986–96
- [129] Hao B, Li H, Lv W, Zhang Y, Niu S, Qi Q, Xiao S, Li J, Kang F and Yang Q 2019 Reviving catalytic activity of nitrides by the doping of the inert surface layer to promote polysulfide conversion in lithium–sulfur batteries *Nano Energy* **60** 305–11
- [130] Zha C, Zhu X, Deng J, Zhou Y, Li Y, Chen J, Ding P, Hu Y, Li Y and Chen H 2020 Facet-tailoring five-coordinated Ti sites and structure-optimizing electron transfer in a bifunctional cathode with titanium nitride nanowire array to boost the performance of Li₂S₆-based lithium–sulfur batteries *Energy Storage Mater.* **26** 40–45
- [131] Zhong Y, Chao D, Deng S, Zhan J, Fang R, Xia Y, Wang Y, Wang X, Xia X and Tu J 2018 Confining sulfur in integrated composite scaffold with highly porous carbon fibers/vanadium nitride arrays for high-performance lithium–sulfur batteries *Adv. Funct. Mater.* **28** 1706391
- [132] Cai D, Zhuang Y, Fei B, Zhang C, Wang Y, Chen Q and Zhan H 2022 Self-supported VN arrays coupled with N-doped carbon nanotubes embedded with Co nanoparticles as a multifunctional sulfur host for lithium–sulfur batteries *J. Chem. Eng.* **430** 132931
- [133] Xiao K, Wang J, Chen Z, Qian Y, Liu Z, Zhang L, Chen X, Liu J, Fan X and Shen Z X 2019 Improving polysulfides adsorption and redox kinetics by the Co₄N nanoparticle/N-doped carbon composites for lithium–sulfur batteries *Small* **15** 1901454
- [134] Fang D, Wang Y, Qian C, Liu X, Wang X, Chen S and Zhang S 2019 Synergistic regulation of polysulfides conversion and deposition by MOF-derived hierarchically ordered carbonaceous composite for high-energy lithium–sulfur batteries *Adv. Funct. Mater.* **29** 1900875
- [135] Sun Z *et al* 2020 Catalytic polysulfide conversion and physiochemical confinement for lithium–sulfur batteries *Adv. Energy Mater.* **10** 1904010
- [136] Qin B, Cai Y, Si X, Li C, Cao J, Fei W, Xie H and Qi J 2021 All-in-one sulfur host: smart controls of architecture and composition for accelerated liquid–solid redox conversion in lithium–sulfur batteries *ACS Appl. Mater. Interfaces* **13** 39424–34
- [137] Niu S *et al* 2020 Freestanding agaric-like molybdenum carbide/graphene/N-doped carbon foam as effective polysulfide anchor and catalyst for high performance lithium sulfur batteries *Energy Storage Mater.* **33** 73–81
- [138] Wang M, Fan L, Wu X, Qiu Y, Guan B, Wang Y, Zhang N and Sun K 2019 Metallic NiSe₂ nanoarrays towards ultralong life and fast Li₂S oxidation kinetics of Li–S batteries *J. Mater. Chem. A* **7** 15302–8
- [139] Zheng H, Li Y, Liu H, Yin X and Li Y 2011 Construction of heterostructure materials toward functionality *Chem. Soc. Rev.* **40** 4506–24
- [140] Song Y, Zhao W, Kong L, Zhang L, Zhu X, Shao Y, Ding F, Zhang Q, Sun J and Liu Z 2018 Synchronous immobilization and conversion of polysulfides on a VO₂–VN binary host targeting high sulfur load Li–S batteries *Energy Environ. Sci.* **11** 2620–30
- [141] Wang Z, Yu K, Feng Y, Qi R, Ren J and Zhu Z 2019 VO₂ (p)-V₂C (MXene) grid structure as a lithium polysulfide catalytic host for high-performance Li–S battery *ACS Appl. Mater. Interfaces* **11** 44282–92
- [142] Fang D *et al* 2021 Combination of heterostructure with oxygen vacancies in Co@CoO_{1–x} nanosheets array for high-performance lithium sulfur batteries *J. Chem. Eng.* **411** 128546
- [143] Zhang H, Zhao Z, Hou Y-N, Tang Y, Liang J, Liu X, Zhang Z, Wang X and Qiu J 2019 Highly stable lithium–sulfur batteries based on p–n heterojunctions embedded on hollow sheath carbon propelling polysulfides conversion *J. Mater. Chem. A* **7** 9230–40
- [144] Ye H and Lee J Y 2020 Solid additives for improving the performance of sulfur cathodes in lithium–sulfur batteries—adsorbents, mediators, and catalysts *Small Methods* **4** 1900864
- [145] Wang Q, Wen Z, Yang J, Jin J, Huang X, Wu X and Han J 2016 Electronic and ionic co-conductive coating on the separator towards high-performance lithium–sulfur batteries *J. Power Sources* **306** 347–53
- [146] Huang J, Zhang Q and Wei F 2015 Multi-functional separator/interlayer system for high-stable lithium–sulfur batteries: progress and prospects *Energy Storage Mater.* **1** 127–45
- [147] Li S, Zhang W, Zheng J, Lv M, Song H and Du L 2021 Inhibition of polysulfide shuttles in Li–S batteries: modified separators and solid-state electrolytes *Adv. Energy Mater.* **11** 2000779
- [148] Liu X, Huang J Q, Zhang Q and Mai L 2017 Nanostructured metal oxides and sulfides for lithium–sulfur batteries *Adv. Mater.* **29** 1601759
- [149] Li M, Wei J, Ren L, Zhao Y, Shang Z, Zhou D, Liu W, Luo L and Sun X 2021 Superwetting behaviors at the interface between electrode and electrolyte *Cell Rep. Phys. Sci.* **2** 100374
- [150] Xiao Z *et al* 2021 Empowering polypropylene separator with enhanced polysulfide adsorption and reutilization ability for high-performance Li–S batteries *Mater. Res. Bull.* **134** 111108
- [151] Shi M *et al* 2022 A Mott–Schottky heterogeneous layer for Li–S batteries: enabling both high stability and commercial-sulfur utilization *Adv. Energy Mater.* **12** 2103657
- [152] Kong Z, Lin Y, Hu J, Wang Y and Zhan L 2022 Phosphorus doped hierarchical porous carbon nanosheet array as an electrocatalyst to enhance polysulfides anchoring and conversion *J. Chem. Eng.* **436** 132719
- [153] Deng C, Wang Z, Wang S, Yu J, Martin D J, Nanjundan A K and Yamauchi Y 2019 Double-layered modified separators as shuttle suppressing interlayers for lithium–sulfur batteries *ACS Appl. Mater. Interfaces* **11** 541–9
- [154] Huang S, Wang Y, Hu J, von Lim Y, Kong D, Guo L, Kou Z, Chen Y and Yang H Y 2019 *In situ*-grown compressed NiCo₂S₄ barrier layer for efficient and durable polysulfide entrapment *npj Asia Mater.* **11** 55
- [155] Wang Q, Liu B, Shen Y, Wu J, Zhao Z, Zhong C and Hu W 2021 Confronting the challenges in lithium anodes for lithium metal batteries *Adv. Sci.* **8** 2101111
- [156] Ren L, Cao X, Wang Y, Zhou M, Liu W, Xu H, Zhou H and Sun X 2023 3D porous and Li-rich Sn–Li alloy scaffold with mixed ionic-electronic conductivity for dendrite-free lithium metal anodes *J. Alloys Compd.* **947** 169362
- [157] Wang Q *et al* 2023 Ultrathin composite Li electrode for high-performance Li metal batteries: a review from synthetic chemistry *Adv. Funct. Mater.* **33** 2213648
- [158] Jinli Q, Longtao R, Xin C, Yajun Z, Haijun X, Wen L and Xiaoming S 2020 Porous copper foam co-operation with thiourea for dendrite-free lithium metal anode *Acta Phys.-Chim. Sin.* **37** 2009020

- [159] Wang Y, Ren L, Liu J, Lu X, Wang Q, Zhou M, Liu W and Sun X 2022 *In situ* construction of composite artificial solid electrolyte interphase for high-performance lithium metal batteries *ACS Appl. Mater. Interfaces* **14** 50982–91
- [160] Yang C, Yin Y, Zhang S, Li N and Guo Y 2015 Accommodating lithium into 3D current collectors with a submicron skeleton towards long-life lithium metal anodes *Nat. Commun.* **6** 8058
- [161] Luo Z, Li S, Yang L, Tian Y, Xu L, Zou G, Hou H, Wei W, Chen L and Ji X 2021 Interfacially redistributed charge for robust lithium metal anode *Nano Energy* **87** 106212
- [162] Xu P *et al* 2020 High reversible Li plating and stripping by *in-situ* construction a multifunctional lithium-pinned array *Energy Storage Mater.* **28** 188–95
- [163] Chen Y, Elangovan A, Zeng D, Zhang Y, Ke H, Li J, Sun Y and Cheng H 2020 Vertically aligned carbon nanofibers on Cu foil as a 3D current collector for reversible Li plating/stripping toward high-performance Li–S batteries *Adv. Funct. Mater.* **30** 1906444
- [164] Zhang C, Lv W, Zhou G, Huang Z, Zhang Y, Lyu R, Wu H, Yun Q, Kang F and Yang Q H 2018 Vertically aligned lithiophilic CuO nanosheets on a Cu collector to stabilize lithium deposition for lithium metal batteries *Adv. Energy Mater.* **8** 1703404
- [165] Xie D, Li H, Diao W, Jiang R, Tao F, Sun H, Wu X and Zhang J 2021 Spatial confinement of vertical arrays of lithiophilic SnS₂ nanosheets enables conformal Li nucleation/growth towards dendrite-free Li metal anode *Energy Storage Mater.* **36** 504–13
- [166] Yan C, Cheng X, Zhao C, Huang J, Yang S and Zhang Q 2016 Lithium metal protection through *in-situ* formed solid electrolyte interphase in lithium–sulfur batteries: the role of polysulfides on lithium anode *J. Power Sources* **327** 212–20
- [167] Bhargava A, He J, Gupta A and Manthiram A 2020 Lithium–sulfur batteries: attaining the critical metrics *Joule* **4** 285–91
- [168] Bonnick P and Muldoon J 2020 The Dr Jekyll and Mr Hyde of lithium sulfur batteries *Energy Environ. Sci.* **13** 4808–33
- [169] Liu B, Fang R, Xie D, Zhang W, Huang H, Xia Y, Wang X, Xia X and Tu J 2018 Revisiting scientific issues for industrial applications of lithium–sulfur batteries *Energy Environ. Mater.* **1** 196–208
- [170] Hu G, Sun Z, Shi C, Fang R, Chen J, Hou P, Liu C, Cheng H M and Li F 2017 A sulfur-rich copolymer@CNT hybrid cathode with dual-confinement of polysulfides for high-performance lithium–sulfur batteries *Adv. Mater.* **29** 1603835
- [171] Wen X, Lu X, Xiang K, Xiao L, Liao H, Chen W, Zhou W and Chen H 2019 Nitrogen/sulfur co-doped ordered carbon nanoarrays for superior sulfur hosts in lithium–sulfur batteries *J. Colloid Interface Sci.* **554** 711–21
- [172] Li J, Chen Y, Zhang S, Xie W, Xu S-M, Wang G and Shao M 2020 Coordinating adsorption and catalytic activity of polysulfide on hierarchical integrated electrodes for high-performance flexible Li–S batteries *ACS Appl. Mater. Interfaces* **12** 49519–29
- [173] Yan Y, Lei T, Jiao Y, Wu C and Xiong J 2018 TiO₂ nanowire array as a polar absorber for high-performance lithium–sulfur batteries *Electrochim. Acta* **264** 20–25
- [174] Liu Y, Sun C, Zhang L, Zheng P, Meng Q, Zhang C, Ye X, Jiang J and Li C M 2022 High S filling and binder-free cathodes enabled by thick arrayed nanoframeworks and subtle interfacial engineering *ACS Appl. Energy Mater.* **5** 1313–21
- [175] Chen S, Zhang J, Wang Z, Nie L, Hu X, Yu Y and Liu W 2021 Electrocatalytic NiCo₂O₄ nanofiber arrays on carbon cloth for flexible and high-loading lithium–sulfur batteries *Nano Lett.* **21** 5285–92
- [176] Zhou J, Yang X, Zhang Y, Jia J, He X, Yu L, Pan Y, Liao J, Sun M and He J 2021 Interconnected NiCo₂O₄ nanosheet arrays grown on carbon cloth as a host, adsorber and catalyst for sulfur species enabling high-performance Li–S batteries *Nanoscale Adv.* **3** 1690–8
- [177] Shan X, Guo Z, Zou Y and Zhao L 2021 Reduced graphene oxide-coated zinc–cobalt oxide nanosheet arrays with N-doped carbon anchored on carbon cloths as cathode materials for high-sulfur-loading Li–S batteries *ACS Appl. Nano Mater.* **4** 11526–36
- [178] Cao Z, Guo J, Jia J, Zhang Z, Yin Y, Yang M and Yang S 2022 *In situ* self-boosting catalytic synthesizing free-standing N,S rich transition metal sulfide/hierarchical CNF-CNT architectures enable high-performance lithium–sulfur batteries *Electrochim. Acta* **422** 140549
- [179] Zhang X, Wei Y, Wang B, Wang M, Zhang Y, Wang Q and Wu H 2019 Construction of electrocatalytic and heat-resistant self-supporting electrodes for high-performance lithium–sulfur batteries *Nano-Micro Lett.* **11** 1–17
- [180] Xiong M, Qian J, Yang K, Chen Z, Mei T, Wang J, Li J, Yu L and Wang X 2020 Efficient polysulfide anchor: brain coral-like WS₂ nanosheets *J. Mater. Sci.* **55** 12031–40
- [181] Jin J, Cai W, Cai J, Shao Y, Song Y, Xia Z, Zhang Q and Sun J 2020 MOF-derived hierarchical CoP nanoflakes anchored on vertically erected graphene scaffolds as self-supported and flexible hosts for lithium–sulfur batteries *J. Mater. Chem. A* **8** 3027–34
- [182] Wang Z, Yu K, Gong S, Du E and Zhu Z 2020 Vanadium based carbide–oxide heterogeneous V₂O₅@V₂C nanotube arrays for high-rate and long-life lithium–sulfur batteries *Nanoscale* **12** 18950–64
- [183] Qiu S, Wang C, Jiang Z, Zhang L, Gu L, Wang K, Gao J, Zhu X and Wu G 2020 Rational design of MXene@TiO₂ nanoarray enabling dual lithium polysulfide chemisorption towards high-performance lithium–sulfur batteries *Nanoscale* **12** 16678–84
- [184] Wang M, Fan L, Tian D, Wu X, Qiu Y, Zhao C, Guan B, Wang Y, Zhang N and Sun K 2018 Rational design of hierarchical SnO₂/1T-MoS₂ nanoarray electrode for ultralong-life Li–S batteries *ACS Energy Lett.* **3** 1627–33
- [185] Qiu Y *et al* 2021 Constructed conductive CoSe₂ nanoarrays as efficient electrocatalyst for high-performance Li–S battery *Rare Met.* **40** 3147–55